Study of the Λ_b Polarization in the DELPHI Experiment at LEP

DELPHI Collaboration

P. Brückman
Institute of Nuclear Physics, Cracow, Poland

Ph.D. thesis

prepared under the supervision of
doc. dr hab. Agnieszka Zalewska

Cracow, 1997

Abstract

This doctoral dissertation presents an experimental measurement of the longitudinal polarization of the Λ_b baryon at LEP e^+e^- collider. The analysis is performed using data collected by the DELPHI experiment. The main theoretical assumptions together with all aspects of the experimental approach are presented.

The Standard Model predicts that at LEP at the Z^0 pole b quarks are produced with a high ($\approx$–0.94) longitudinal polarization. The possible transfer of this polarization to the ground baryonic state Λ_b makes an important prediction of the HQET. Therefore, measurement of the Λ_b polarization would give an important hint about heavy quark hadronization processes and heavy baryon properties.

The polarization is experimentally accessible by measuring the charged lepton and neutrino energy spectra from the Λ_b semileptonic decays. Moreover, since the neutrino is predicted to be the decay product most sensitive to polarization, its energy reconstruction via the hemisphere missing energy is essential for the presented method.

From the data sample of $\approx$3 million hadronic Z^0 decays collected by DELPHI in the years 1993–1995 271$\pm$22 Λ_b semileptonic decay candidates are selected using Λ^0 lepton correlations. The measured polarization is:

$$P_{\Lambda_b} = -0.48^{+0.35}_{-0.27}(\text{stat.})^{+0.15}_{-0.13}(\text{syst.})$$

Contents

1 Introduction 1
2 The DELPHI spectrometer 6
2.1 Apparatus 6
2.2 Lepton identification 11
2.3 Collected data 12
3 Theoretical considerations related to the Λ_b polarization 13
3.1 Polarization of fermions from $e^+e^- \to Z^0 \to f\bar{f}$ 18
3.2 b quark hadronization in the HQET approximation 19
3.3 Possible depolarization effects 20
3.4 SM description of the semileptonic decay $\Lambda_b^0 \to \Lambda_c^+ l\bar{\nu}$ 21
4 Experimental approach to the Λ_b polarization measurement (possibilities and limitations) 25
4.1 Choice of the decay channel 25
4.2 Observables 26
4.3 Polarized Λ_b decays in the simulation 30
5 Analysis procedure 32
5.1 Global event selection 33
5.2 Λ_b signal selection 33
5.3 Background estimation and subtraction 42
5.4 B^0 signal selection 49
5.5 Neutrino energy reconstruction 51
6 Polarization measurement results and error estimation 59
6.1 Measured value of the Λ_b polarization 59
6.2 Statistical error 61
6.3 Systematic uncertainties 62
6.4 Consistency check using B mesons 66
6.5 Comparison with the ALEPH measurement of P_{Λ_b} 67
6.6 Implications of the result 70
7 Conclusions 72
Acknowledgements 73
Bibliography 74
List of Figures 80
List of Tables 82

1 Introduction

The dissertation presented here shows the methodology and results of an experimental measurement of the Λ_b baryon polarization at the LEP e^+e^- collider. The study is performed using data collected by the DELPHI experiment. The first concept based on the theoretical predictions was outlined in 1995 [1]. Then after an extensive experimental study the preliminary results together with the status of the Λ_b polarization measurement from the other LEP experiments were presented during the Warsaw ICHEP'96 conference [2]. Now we present a complete experimental approach resulting in a well controlled physical measurement.

The DELPHI detector is installed at the LEP (**L**arge **E**lectron-**P**ositron) collider at CERN where it has operated since 1989. The DELPHI apparatus will be described in more detail in section 2. The LEP machine [3, 4, 5] is the world's largest particle

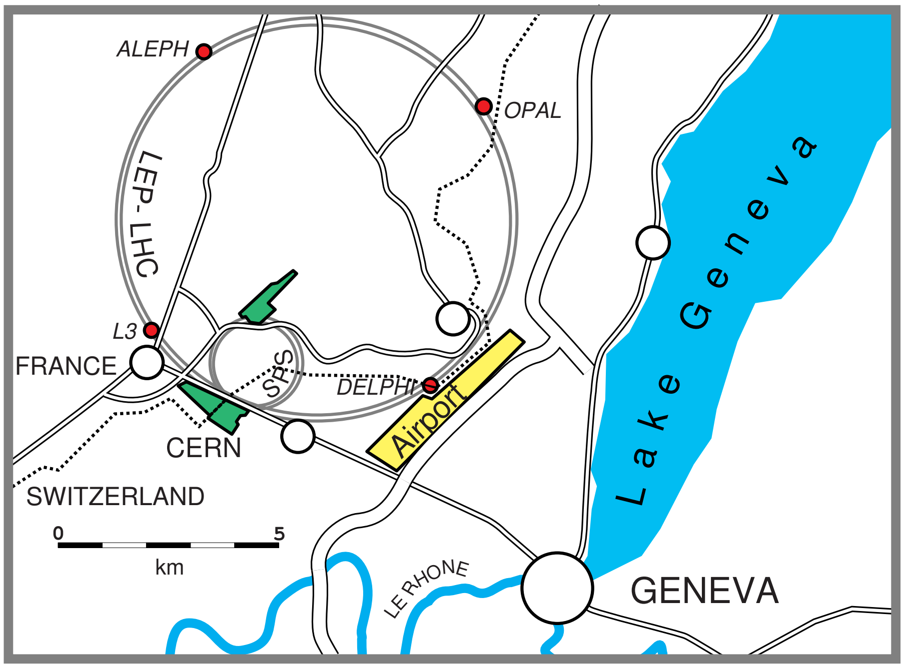

Figure 1: Schematic map of the LEP collider situation [6].

accelerator (26.7 km in circumference some 100 meters underground) and is situated on the French-Swiss border near Geneva, Switzerland (Fig. 1). Since 1989 and during the following six years (till 1995) the e^+e^- machine operated at the Z^0 resonance, i.e. with a center of mass energy around the Z^0 boson mass ($E_{\rm CM} \cong m_Z$)[1]. This LEP operating period is customarily called LEP1. The first tests of the higher energy regime started in 1995. Since then LEP has been operating at higher energies aiming to explore $W^{\pm}$ physics and possibly to find evidence for new phenomena beyond the Standard Model. This period is called LEP2. Since the presented analysis is strictly related to physics at the Z^0 pole hereafter we will refer exclusively to the LEP1 operating period.

During the LEP1 scan periods the Z^0 mass itself as well as the width of the Z^0 resonance were measured by the LEP experiments with a very high precision [7, 8, 9, 10][2]:

$$\begin{aligned} m_Z &= 91.1863 \pm 0.0020 \text{ GeV} \\ \Gamma_{Z\,\rm tot} &= 2494.6 \pm 2.7 \text{ MeV} \end{aligned} \tag{0.1}$$

LEP together with SLAC in Stanford (USA) [11, 12] are currently the world's best places to explore the weak neutral current coupling to quarks and leptons. The LEP circular collider provides collisions of unpolarized e^+e^- beams with a high luminosity[3]. SLAC in turn being a linear accelerator offers a much lower interaction rate but is able to provide highly polarized beams which gives particular advantages for electroweak measurements. Effectively the two machines give compatible sensitivity to most of the electroweak parameters at the Z^0 resonance. Therefore, throughout this paper we will rather quote combined results from all LEP experiments and the SLD experiment at SLAC. For some measurements concerning b physics results from the CDF experiment at the Tevatron $\rm p\bar{p}$ collider will be added as well. The LEP($\oplus$SLD$\oplus$CDF) combined results quoted here are the best compilations of results from the ALEPH, DELPHI, L3 and OPAL (SLD, CDF) experiments taken from [13], [14], [15], [16] and [17].

At LEP an e^+e^- annihilation can proceed either via a highly virtual γ particle or via a Z^0 mediating weak neutral interactions. Both intermediate bosons subsequently decay into a fermion pair $f\bar{f}$. The Standard Model formulae governing these processes will be discussed in section 3. At the center of mass energy close to the Z^0 mass (the Z^0 resonance) the cross-section is dominated by the Z^0 exchange by almost three orders of magnitude. Therefore, it is often assumed that events observed at LEP1 originate exclusively from Z^0 decays. We say that a Z^0 decays hadronically when it produces a $q\bar{q}$ pair which subsequently hadronizes and cascades into jets of particles. This category contains also events with one or more hard gluons radiated from the final state $q\bar{q}$. The latter lead to events containing three or more jets originating from the initial partons ($q\bar{q}g$, $q\bar{q}gg$, etc.). Hadronic events account for 70% of all Z^0 decays ($\Gamma_{\rm had}/\Gamma_{\rm tot}$ = (69.90 ±

[1]Except for the years 1992 and 1994 years LEP was operating at variable energies scanning the Z^0 resonance. The main scan scheme was: $E_{\rm CM} = m_Z$, $m_Z - 2$GeV and $m_Z + 2$GeV.

[2]The latest preliminary results quoted in [13] are: $m_Z = 91.1867 \pm 0.0020$ GeV and $\Gamma_{Z\,\rm tot} = 2494.8 \pm 2.5$ MeV

[3]The maximum integrated luminosity per LEP experiment in any year was attained in 1994 when it reached a value of 64 $\rm pb^{-1}$ [18]

0.15)% [19]). Apart from hadronic events Z^0 can also decay into a pair of charged leptons $e^+e^- \to Z^0 \to l^+l^-$, where l denotes either e, μ or τ ($\Gamma_l/\Gamma_{\rm tot} \cong 10\%$) or a pair of neutrinos $e^+e^- \to Z^0 \to \nu_l\bar{\nu}_l$ ($\Gamma_\nu/\Gamma_{\rm tot} \cong 20\%$). Neutrino events however cannot be directly observed since they lead to empty events in the detector apparatus. They are often called "invisible" Z^0 decays. The Z^0 partial widths measured at LEP are as follows:

$$\begin{aligned} \Gamma_{\rm had} &= 1743.6 \pm 2.5 \text{ MeV} \\ \Gamma_{e,\mu,\tau} &= 251.5 \pm 0.3 \text{ MeV} \\ \Gamma_{\rm inv.} &= 499.5 \pm 2.0 \text{ MeV} \end{aligned} \tag{0.2}$$

LEP is an excellent accelerator for exploring reactions in which b quarks take part [20]. Z^0 has a large coupling to b quarks. A $b\bar{b}$ pair is produced in a high fraction of all Z^0 decays (BR($Z^0 \longrightarrow b\bar{b}$) = (15.45 $\pm$ 0.21)% [19]) and amounts to 22% of Z^0 decays into $q\bar{q}$ pairs. The fraction of so called b events relative to the total number of hadronic Z^0 decays is an important Standard Model prediction which has been confirmed by experimental measurements at LEP and SLAC. The combined LEP$\oplus$SLD result for $R_b = \Gamma_{Z\to b\bar{b}}/\Gamma_{Z\to \rm hadrons}$ is: $R_b = 0.2170 \pm 0.0009$. The b hadrons produced at LEP have large boost, making them more easily identifiable in the relatively clean environment of e^+e^- collisions.

The high energy p$\bar{\rm p}$ colliders produce b-hadrons in large numbers (e.g. Tevatron at Fermilab) but proton interactions lead to high multiplicities and hence a huge combinatorial background to any exclusive b signal. However, due to the very high production rate hadron colliders can also give valuable contribution to the b spectroscopy.

In particular the analysis of baryons containing a heavy quark b has been of growing interest to all LEP experiments over the last years. So far only the lightest baryonic state of this type – Λ_b – has been well explored. The Λ_b baryon consists of three valence quarks (bud). The light pair (ud) forms a light diquark of a total spin $S = 0$. From the quark model the Λ_b quantum numbers are predicted to be: $I(J^P) = 0(\frac{1}{2}^+)$. This prediction however has not yet been experimentally confirmed. The first observation of Λ_b was made by the UA1 collaboration in 1991 [21] and its mass was determined to be $(5640 \pm 50 \pm 30)$MeV/c^2. Subsequently, the large majority of results on b-baryons have come from the LEP experiments. The first evidence of b-baryon production was reported already in the early years of the LEP operation [22, 23, 24]. Later, its mass was determined with better accuracy using fully reconstructed Λ_b decays [25, 26]. Combining the first UA1 number with the measurements at LEP gives the result: $m_{\Lambda_b} = 5639 \pm 16$ MeV/c^2. Recently, by far the best measurement of the Λ_b mass has been reported by the CDF collaboration. Reconstructing $\approx$20 events where $\Lambda_b \to J/\Psi\Lambda^0$ they determine the Λ_b mass: $m_{\Lambda_b} = 5621 \pm 4 \pm 3$ MeV/c^2 [14]. A lot of effort has also been put into the measurement of the mean b-baryon lifetime and its comparison with the meson sector. The LEP$\oplus$SLD$\oplus$CDF combined results on b hadron lifetimes are:

$$\begin{array}{ll} \tau_{B^0} = 1.55 \pm 0.04 & \multirow{2}{*}{[27, 28, 29, 30, 31, 32, 33, 34, 35]} \\ \tau_{B^+} = 1.65 \pm 0.04 & \\ \tau_{B_s^0} = 1.52 \pm 0.07 & [36, 37, 38, 39, 40, 41, 42] \\ \tau_{\Lambda_b} = 1.21 \pm 0.06 & [43, 44, 45, 46, 47, 48] \end{array} \tag{0.3}$$

Here all quoted baryon analyses select the Λ_b signal as the easiest and most populated baryon representative.

Recently first evidence for the strange b-baryon Ξ_b from Ξ lepton correlations have been reported at LEP [49, 50, 51]. However, the hope for a mass measurement using full reconstruction is small.

The DELPHI collaboration has also found the first evidence for the Σ_b and Σ_b^* baryons [52]. The signal was found correlating a soft pion with the baryon enriched inclusive b vertices ($\Lambda_b + \pi^{\pm} \rightarrow \Sigma_b, \Sigma_b^*$).

Already the lightest baryonic ground state Λ_b gives a unique possibility of investigating some phenomena inaccessible in case of the far more frequently occurring heavy mesons. One such interesting effect is a possibility of a strong longitudinal polarization of the Λ_b, this being a direct consequence of the polarization of primary b quark coming from a Z^0 decay. Polarization reflects the dynamics of the reaction and is defined as an asymmetry in the spin orientation of the particle. It will be precisely defined in chapter 3. The Standard Model predictions for the primary quark polarization produced in $e^+e^- \rightarrow Z^0 \rightarrow q\bar{q}$ are presented in section 3.1. Then the discussion of the polarization transfer to the final state hadron together with possible sources of depolarization follows in sections 3.2 and 3.3. Finally, the detailed discussion of the dynamics of the semileptonic weak decay of a polarized b quark is given in section 3.4.

The measurement of the Λ_b polarization is based on the asymmetry in the angular distributions of the charged lepton and neutrino induced by the b polarization. The precise description of the measurement methodology together with the justification of the chosen experimental approach is presented in section 4.

Section 5 contains a detailed account of the analysis procedure. It describes Λ_b signal selection (5.2), discusses existing background sources (5.3) and finally throws light on the crucial experimental difficulty of reconstructing the energy of the escaping and undetectable neutrino particle which turns out to carry most of the polarization information (5.5). Subsection 5.4 describes the selection of the auxiliary signal of semileptonic B^0 decays used as an additional cross-check of the consistency of neutrino energy reconstruction.

The measurement result is presented in section 6.1. The following sections 6.2 and 6.3 contain a discussion of the statistical error and the systematic uncertainty respectively. Next, in section 6.4 we present results of the identical analysis performed on B mesons. The obtained result being compatible with zero confirms consistency of the presented experimental method and in particular proves correctness of the neutrino energy reconstruction. In section 6.5 we present the ALEPH results on the Λ_b polarization. The comparison and compilation of the ALEPH and DELPHI results is done in addition. Section 6.6 gives possible interpretations of the obtained results when combined with other measurements and theoretical predictions.

The conclusions are given in section 7.

2 The DELPHI spectrometer

DELPHI (**DE**tector with **L**epton, **P**hoton and **H**adron **I**dentification) is a general purpose detector for e^+e^- collider physics, designed to provide high granularity over a 4π solid angle, and allowing powerful particle identification. It is installed at the LEP e^+e^- collider at CERN, near Geneva. The DELPHI detector has been operational since 1989.

This chapter is based on two publications [53],[54] concerning components of the DELPHI spectrometer and its performance. Here we will concentrate on those subdetectors which are essential for the presented analysis i.e. tracking detectors, calorimeters and lepton identification devices. Additionally we briefly present the RICH detectors which are the most interesting ones and specific for DELPHI although do not directly contribute to this analysis.

2.1 Apparatus

In the standard DELPHI coordinate system the z axis lies along the electron beam direction, the x axis points towards the center of LEP and the y axis point upwards. The polar angle measured from the z axis is called θ and the azimuthal angle around z is called ϕ; the radial coordinate is $R = \sqrt{x^2 + y^2}$. The detector consists of a cylindrical section covering the "barrel" region of θ (typically $40° - 140°$) and two endcaps covering the "forward" regions. The angular coverage of the "forward" subdetectors go typically down to $\theta = 10°$ (or $\theta = 170°$). Figure 2 schematically shows the present layout of the barrel part and of one endcap. The central part of the detector consists of tracking detectors and specialized hadron identification devices – RICHes. In this region, called the central tracking volume, a highly uniform magnetic field of 1.23 T parallel to the z axis is provided by the superconducting solenoid. The electromagnetic calorimeter is placed between tracking detectors and the solenoid. Outside the superconducting solenoid there are: hadronic calorimeter serving additionally as a magnetic field return yoke and the outermost detectors – muon chambers placed inside and outside the hadronic calorimeter.

Tracking detectors

Charged particle reconstruction is performed by the tracking detectors. They are designed to reconstruct a charged particle path by probing its position at many points along the trajectory. The charged particle momentum is determined thanks to the presence of the strong magnetic field in the tracking volume. Charged particles move along a helix whose radius R_h in the xy projection depends on their transverse momentum. The particle momentum is related to its trajectory curvature by the formula $p = 0.003 \times B \times R_h/\sin\theta$, where B is the magnetic field in Tesla, θ denotes the polar angle of the particle momentum and R_h is in cm. The tracking in the barrel part of

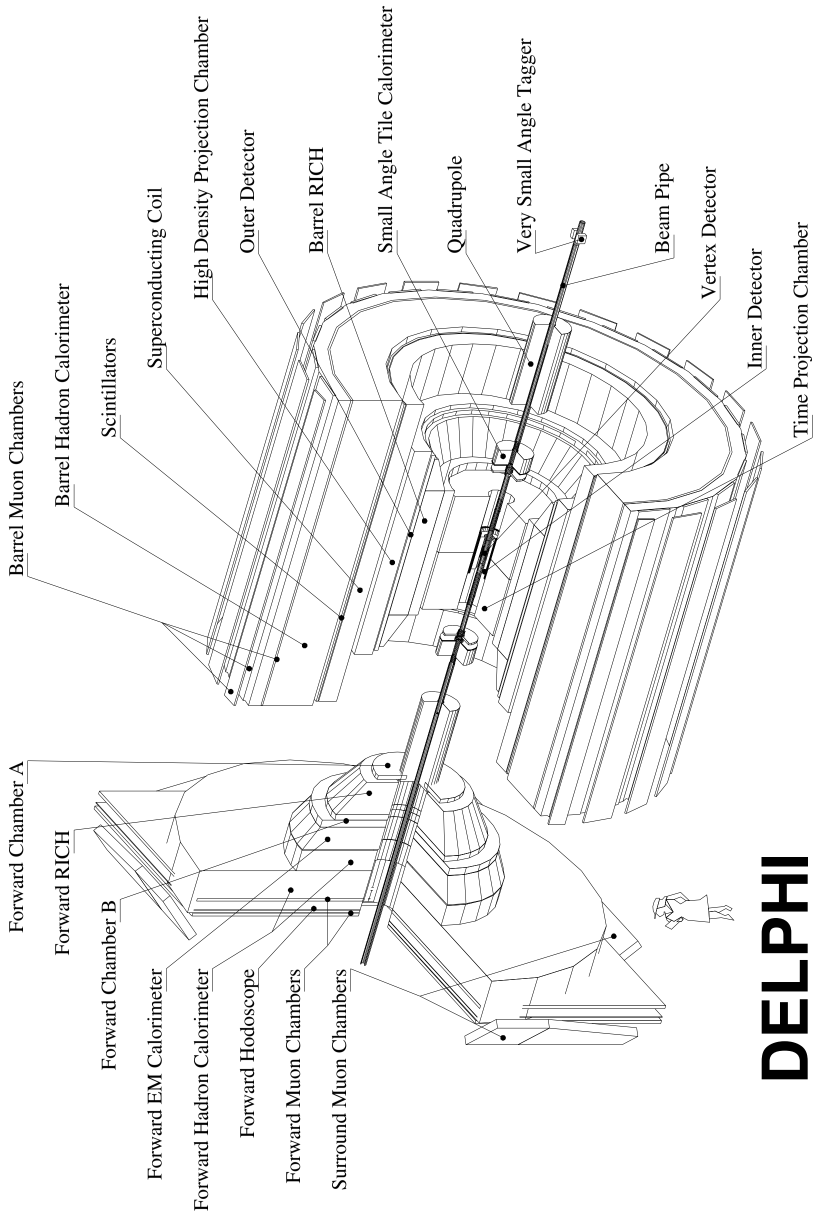

Figure 2: Schematic layout of the DELPHI spectrometer [57].

DELPHI is done by the Vertex Detector (VD), the Inner Detector (ID), the Time Projection Chamber (TPC) and the Outer Detector (OD). In the forward region there are two tracking devices; Forward Chambers A (FCA) and Forward Chambers B (FCB).

The VD [55, 56] is the innermost subdetector of the DELPHI apparatus. It consists of three coaxial layers of AC coupled silicon strip detectors at average radii of 6.3, 9.0 and 10.9 cm. Each layer covers the full azimuthal angle with overlaps between adjacent modules. There are 4 detectors along the beam direction in each module. The polar coverage of the VD corresponds approximately to the barrel part of DELPHI. For polar angles of $44° \leq \theta \leq 136°$ a particle crosses all three layers. Until 1993 VD gave only the $R\phi$ information from single-sided detectors. In 1994 the first layer (Closer) and the third layer (Outer) of the vertex detector were equipped with double-sided modules, having additional orthogonal strips on the opposite side of plaquettes. In this way the VD gained an additional capability to measure the z coordinate. The $R\phi$ readout pitch is 50 μm and is uniform for the whole detector. The single hit precision was found to be 7.6 μm. The z coordinate readout pitch is not identical for the whole detector and ranges from 42 μm to 84 μm. The single hit precision of the z measurement is a function of the incidence angle θ and varies from 9 μm to over 30 μm. The VD is the most precise tracking device of DELPHI. It makes possible a precise reconstruction of the primary interaction vertex and eventually the separation of secondary vertices resulting from the decays of long-living hadrons containing b and c quarks as well as the heavy lepton τ (i.e. lifetimes of the order of 0.3—1.6 ps).

The ID should be considered separately in the periods until the end of 1994 and from 1995 on. During the 94/95 winter shutdown the "standard" Inner Detector was replaced by a completely new longer device. The "standard" ID is composed of two independent parts. The inner drift chamber (jet chamber) provides up to 24 $R\phi$ points per track between radii of 12 and 23 cm. The jet chamber is surrounded by 5 MWPC layers providing both $R\phi$ readout (wires) and Rz information (cathode strips). The MWPC information is used mainly for triggering but also provides valuable Rz measurements and gives the possibility of resolving the left/right drift ambiguities inherent in the jet chamber. The polar angle acceptance of the ID is $30° \leq \theta \leq 150°$. The single track element reconstructed in the jet chamber is measured with $\sigma(R\phi)$=50 μm and the two track resolution is about 1 mm. A single MWPC layer gives a z precision of between 0.5 and 1 mm depending on θ. Since 1995 a new longer ID has been operational. The new inner drift chamber has exactly the same wire configuration as the previous one while the surrounding proportional chambers have been replaced by 5 layers of straw tube detectors. The straw tubes have the same functionality as the old MWPC trigger layers although they do not provide any z measurement. The new longer ID has a polar angle acceptance of $15° \leq \theta \leq 165°$ and a single track element precision of $\sigma(R\phi)$=40 μm.

The TPC serves as the main tracking device of the DELPHI spectrometer. It provides up to 16 three-dimensional space points per particle trajectory at radii of between 35 and 111 cm. Its polar acceptance covers angles down to $20° \leq \theta \leq 160°$ for tracks giving at least three space points. Both end-plates of the TPC are divided into six azimuthal sectors, each with 192 sense wires and 16 circular pad rows with constant spacing. Sense wires together with pad rows provide the measurement of two dimensions in the $R\phi$ plane while the drift time determines the z position of the track trajectory. The single point precision in the $R\phi$ plane is 250 μm and 880 μm in the Rz plane. The two point resolution is about 1cm in both directions.

The OD consists of 5 layers of drift tubes operated in the limited streamer mode. It is located between radii 197 and 206 cm. The tubes provide the $R\phi$ measurement with a single point precision of 110 μm. Additionally, three layers are equipped to read the z coordinate by timing the signals at the ends of anode wires. This technique gives a z precision of 3.5 cm.

In the endcaps there are two tracking detectors: FCA and FCB. FCA drift chambers are mounted at a distance of about 160 cm in $|z|$ from the interaction point. The chamber covers polar angles of $11° \leq \theta \leq 32°$ and $148° \leq \theta \leq 169°$. FCA gives the precision of the reconstructed track element of 8.5 mrad in θ and 24 mrad in ϕ. FCB is a drift chamber at an average distance of $|z|$=275 cm from the interaction point. The sensitive area of the chamber covers polar angles $11° \leq \theta \leq 36°$ and $144° \leq \theta \leq 169°$. The precisions achieved on the parameters of the reconstructed track elements are 3.5 mrad in θ and 4.0/sinθ mrad in ϕ.

RICH detectors

The Ring Imaging Cherenkov (RICH) detectors are mounted both in the barrel (BRICH) and the forward region (FRICH) of DELPHI and cover almost the whole 4π solid angle. They combine liquid and gas radiators to identify charged particles over most of the momentum range at LEP1. Their capability to distinguish particles with different masses is used mainly for the charged hadron identification. The charged lepton identification will be described elsewhere in this chapter. The liquid radiator is used for the particle identification in the momentum range from 0.7 to 8 GeV/c. The gas radiator gives identification information in the range between 2.5 and 25 GeV/c. The RICH detectors are based on the Cherenkov light emission principle. Charged particles traversing a dielectric medium faster than the speed of light in that medium radiate photons onto a cone of definite angle θ_c around its momentum direction. The emission angle depends on the mass M and momentum p via the relation $\cos\theta_c = 1/n \times \sqrt{1 + M^2/p^2}$, where n is the refractive index of the radiator medium. The number of photons emitted per unit length is proportional to $\sin^2\theta_c$. Particle identification in RICH detectors relies on the reconstructed Cherenkov angle and number of photons associated to a track. The fact that particles below the Cherenkov threshold do not emit light is also used for the identification ("veto identification").

Calorimeters

Calorimeters serve for the detection of neutral hadrons and γ particles via the total attenuation of their energy. The measurement giving both the particle energy and approximate position relies on the detection of nuclear and electromagnetic cascades induced by it while passing through matter. There are two main kinds of calorimeters in the DELPHI spectrometer; electromagnetic calorimeters (HPC in the barrel part and FEMC in the forward) and hadron calorimeters (HAC). Electromagnetic calorimeters serve additionally as a main source of electron identification (see the following paragraph).

The barrel electromagnetic calorimeter, HPC (High density Projection Chamber), consists of 144 modules arranged in 6 rings inside the magnetic field. Each ring is composed of 24 modules coaxially arranged around the beam axis with an inner radius of 208 cm and an outer radius of 260 cm. Each HPC module is a small TPC with layers of high density material in the gas volume. These layers are made of lead wires which serve not only as converter material but provide the drift field as well. The total converter thickness is $18X_0/\sin\theta$. The relative precision on the measured energy can be parameterized as $\sigma(E)/E = 0.043 \oplus 0.32/\sqrt{E}$ where E is expressed in GeV. The HPC technique provides also very good spatial resolution. The angular precisions for high energy photons are 1.7 mrad in the azimuthal angle ϕ and 1.0 mrad in the polar angle θ.

The Forward ElectroMagnetic Calorimeter (FEMC) consists of two arrays of 4532 Cherenkov lead glass blocks; the front faces are placed at $|z| = 284$ cm, covering the polar angles $8^\circ \leq \theta \leq 35^\circ$ and $145^\circ \leq \theta \leq 172^\circ$. The glass blocks have depths of 40 cm corresponding to 20 radiation lengths. The Cherenkov light induced by the charged particles in the shower is read out by a single stage photomultiplier (triode) designed to operate inside the DELPHI magnetic field. The relative precision on the measured energy can be parameterized as $\sigma(E)/E = 0.03 \oplus 0.12/\sqrt{E} \oplus 0.11/E$ where E is in GeV. For neutral showers of energy larger than 2 GeV, the average precision on the reconstructed hit position in x and y projected to $|z|$=284 cm is about 0.5 cm.

The Hadron CALorimeter (HCAL) is installed in the return yoke of the DELPHI solenoid. It is made of a barrel section which consists of 24 modules and two endcaps, each consisting of 12 sectors. The whole HCAL covers almost the full solid angle: $11^\circ \leq \theta \leq 169^\circ$. It has a "sandwich" structure. More than 19,000 limited streamer tubes are installed in the 18 mm wide slots between the 50 mm thick iron plates. In the barrel region ($52^\circ \leq \theta \leq 128^\circ$) the energy precision in the hadron calorimeter was found to be $\sigma(E)/E = 0.21 \oplus 1.12/\sqrt{E}$ where E is expressed in GeV. The granularity of the HCAL is relatively poor. The single channel readout cells have the angular dimensions of $\Delta\phi = 3.75^\circ$ and $\Delta\theta = 2.96^\circ$ in the barrel and $\Delta\theta = 2.62^\circ$ in the end caps.

2.2 Lepton identification

Muon identification

The identification of muons is based on the information coming from the muon chambers (MUC). These are set of drift chambers with the three-dimensional readout situated at the periphery of the DELPHI apparatus. In the barrel they consist of three layers each including two planes of active chambers. In the endcaps these are two layers containing two chamber planes each. The iron of the hadron calorimeter ($\approx$1 m thick) provides a filter which gives a first level separation between muons and hadrons. Most hadrons are stopped by this material, whereas all muons of momenta above 2 GeV/c are expected to penetrate to the muon chambers.

Charged particle tracks, reconstructed in the central detectors, are extrapolated through the solenoid and the iron of HCAL to the muon chambers. The extrapolation is done referring to the map of the return magnetic field along the track path and the covariance matrix of track parameters is also propagated taking into account multiple scattering. Then a χ^2 based association between extrapolated tracks and hits in MUC is done. All tracks having at least 1 associated hit are considered as potential muon candidates. The further detailed tagging is based on number of associated hits in muon chambers and two χ^2 discriminators; χ^2_{global} – global χ^2 of the track fit to the associated hits in MUC and χ^2_{ex} – the χ^2 contribution from the track extrapolation alone. The final identification flags are set in case the above variables satisfy certain criteria defined for each tag level.

The so called Standard tag gives the tagging efficiency of $(86.1 \pm 0.2)\%$ with the misidentification probability $(0.7 \pm 0.1)\%$ and the Loose one has an efficiency $(94.8 \pm 0.1)\%$ with misidentification of $(1.5 \pm 0.1)\%$.

Electron identification

The electron identification in DELPHI is less performant than the muon identification since the situation is complicated by electromagnetic interactions in front of the electromagnetic calorimeters (HPC in barrel and FEMC in the forward region). In the barrel region material amounts to about $0.8X_0/\sin\theta$ and in the forward region is even larger.

The electron identification in barrel region is performed using two independent and complementary measurements, the dE/dX measurement of the TPC and the energy deposition in the HPC. The comparison of the charged track momentum (measured from the track curvature) with the energy of the associated electromagnetic shower gives the powerful identification tool. Having corrected for the multiple scattering losses and nonlinearities in the calorimeter the electron energy deposit should be equal to its momentum while hadrons can give only fractional deposits. The calorimetric identification is based on the χ^2 probability of the extrapolated track fit to the longitudinal profile of the nearest electromagnetic shower. Both shower position and direction as well as the energy deposited and the shape of the shower contribute to the global χ^2. The totally independent dE/dX measurement in the TPC leads to the additional $e-\pi$ separation. For low momentum tracks (below 4.5 GeV/c) the separation is better than 3σ and still above 2σ for momenta up to 20 GeV/c.

The electron identification in the forward part of DELPHI is also based on the comparison between track momentum and the electromagnetic energy deposited in the associated shower. Here instead if HPC the calorimetric information is provided by the FEMC. Because of the limited geometrical acceptance the dE/dX information from the TPC plays minor role in the forward region identification.

The Standard electron tag gives the efficiency of about 55% with ≈0.4% probability of hadron misidentification. The Loose tag is about 80% efficient while the misidentification probability is ≈1.6%.

2.3 Collected data

The DELPHI detector has been operational since 1989. The presented analysis is based on the data collected during the LEP1 operation period. The number of hadronic Z^0 decays recorded by the DELPHI experiment each year at LEP1 are summarized in Table 1. In practice data coming from 1989 and 1990 are almost never taken into account because of low statistics and the lack of precise detector calibration. Furthermore, the 1991 and 1992 data has been excluded from the analysis because they still exist only in an old format making them incompatible with the newly developed algorithm to reconstruct the total hemisphere energy which has been used here. Therefore finally in the presented analysis we have used data collected in the years 1993 to 1995 amounting to a total number of about 2,989,000 hadronic Z^0 decays.

Year	1989	1990	1991	1992	1993	1994	1995	Total
Off peak	4K	30K	52K	—	243K	—	236K	617K
Total	13K	125K	275K	751K	755K	1484K	750K	4153K

Table 1: Number of hadronic Z^0 decays recorded by DELPHI in each year of operation of LEP1. The statistics recorded at energies off the Z^0 resonance peak during scan periods are given separately [54].

3 Theoretical considerations related to the Λ_b polarization

In this chapter we will review the very basic electroweak relations related to physics at the Z^0 pole and then will concentrate on the theoretical predictions concerning our analysis. The production of polarized fermions from the Z^0 decay, possible transfer of the polarization to hadrons and the semileptonic decay of the Λ_b baryon will be discussed.

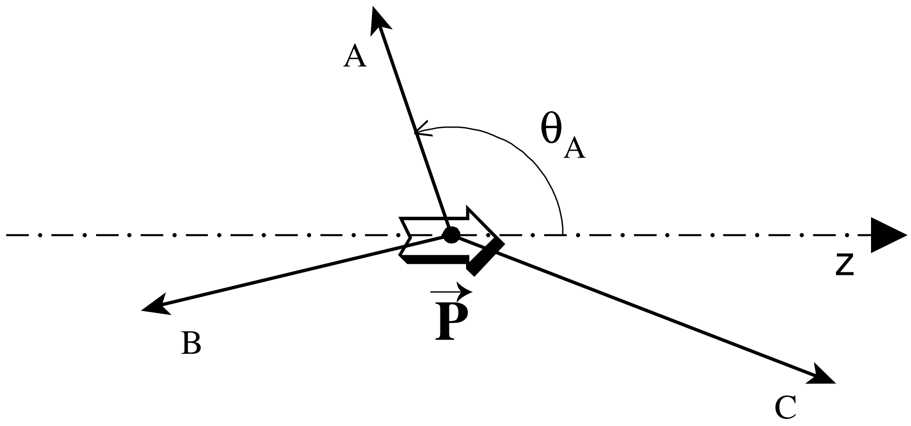

Figure 3: Definition of the reference frame and the θ angle in the rest frame of the decaying polarized particle. The z axis is equivalent to the spin quantization axis.

Polarization is an asymmetry in the spin orientation. It is defined as:

$$P = \frac{\Gamma(+s) - \Gamma(-s)}{\Gamma(+s) + \Gamma(-s)} \tag{0.4}$$

where $\Gamma(+s)$ and $\Gamma(-s)$ are the probabilities to find the particle with the positive and negative spin projection on the quantization axis respectively. Polarization reflects the dynamics of the reaction in which a polarized particle is produced and can be generated only in the parity violating weak processes. Analogously, only the parity violating weak decays can give asymmetries in the angular distribution of the decay products. These are the only observable traces of the polarization. The asymmetry defined in the decaying particle rest frame is described by the formula:

$$\frac{d\Gamma}{d\cos\theta} = \frac{1}{2}[1 + P\alpha(x)\cos\theta] \tag{0.5}$$

where the reference frame and the θ angle are defined as shown in Fig. 3 and x is a variable related to the energy of the decay product. The detailed discussion of the dynamics of the semileptonic weak decay of a polarized b quark is given in section 3.4.

The Standard Model (SM) [58] is based on the rather complicated gauge symmetry known as $SU_3 \oplus SU_2 \times U_1$. The modern theory of strong interactions (QCD) is associated with the SU_3 group while electroweak sector is described by the combined symmetry group $SU_2 \times U_1$. There are three different bosons mediating electroweak interactions and there are three corresponding fermion–boson vertices. Exchange of photons (Fig. 4a)

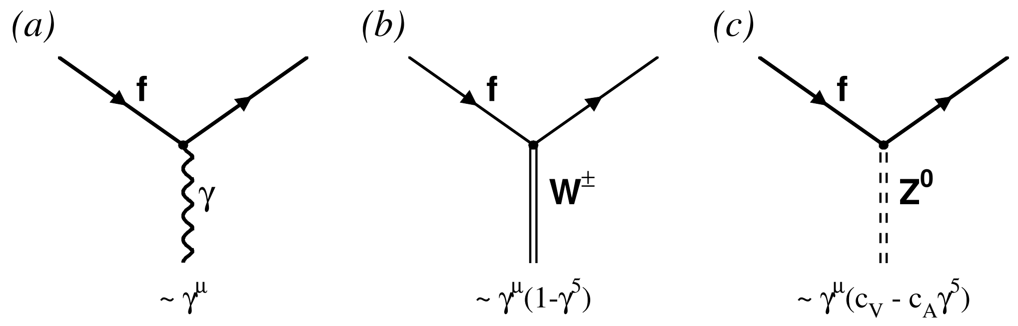

Figure 4: Three principal fermion vertices of the electroweak theory; (a) electromagnetic interaction; (b) flavour changing weak interaction; (c) flavour conserving weak interaction.

is responsible for the electromagnetic interactions and has a vector (**V**) character. It means that it couples with the same strength to the right-handed and left-handed fermions and hence conserves the parity. Since in the limit of high momentum (or vanishing fermion mass: $m_f \to 0$) handness becomes identical with helicity we may say that electromagnetic interactions do not distinguish helicities and thus cannot generate any polarization. The electromagnetic coupling constant is $q^f = eQ^f$ where e is the proton charge and Q^f gives the fermion charge in the units of e. $W^{\pm}$ and Z^0 mediate the flavour-changing charge current (Fig. 4b) and the flavour-conserving neutral current (Fig. 4c) weak interactions respectively. $W^{\pm}$ exchange is described by so called (**V-A**) coupling which means that $W^{\pm}$ couples exclusively to the left-handed fermions. Such an interaction maximally violates the parity and hence generates polarization and can

$\sin^2\Theta_W = 0.23$	c_V	c_A
$\nu_e,\ \nu_\mu,\ \nu_\tau$	1	1
$e,\ \mu,\ \tau$	$-1 + 4\sin^2\Theta_W = -0.080$	-1
$u,\ c,\ t$	$1 - \frac{8}{3}\sin^2\Theta_W = 0.387$	1
$d,\ s,\ b$	$-1 + \frac{4}{3}\sin^2\Theta_W = -0.693$	-1

Table 2: Numerical values of the vector and axial-vector couplings to the weak neutral current for different fermion species assuming $\sin^2\Theta_W = 0.23$. Note that there are common couplings for all three fermion families.

give angular asymmetries in the decays of polarized particles. All left-handed fermions couple to the $W^\pm$ with the same strength g. It is related to the electromagnetic coupling e via the electroweak mixing angle Θ_W: $g = e/\sin\Theta_W$. The Z^0 boson has the most complicated coupling to fermions which is a linear combination of vector (**V**) and axial-vector (**A**) currents. The admixtures of **V** and **A** coupling are different for different fermion species and are denoted by c_V and c_A respectively. Their numerical values are summarized in Table 2. Since the $W^\pm$ bosons are not involved in the primary interaction at LEP1 we will concentrate in the following on the electromagnetic and the weak neutral currents only.

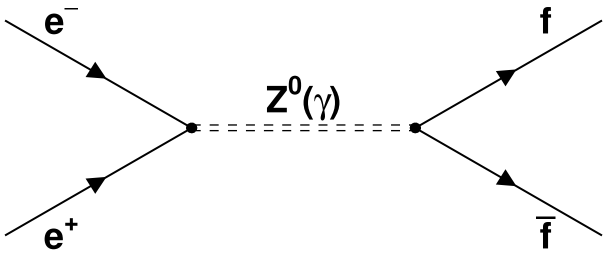

Figure 5: A principal diagram representing the Born approximation of the e^+e^- interaction at LEP.

LEP1, which operates at the Z^0 resonance, has a unique[1] opportunity to investigate spin physics via the longitudinal polarization of fermions produced in the Z^0 boson decay. In the first approximation the e^+e^- annihilation can go either to a highly virtual γ particle or to a weak interaction neutral boson Z^0 as shown in Fig. 5. In the continuum region, i.e. at the center of mass energy away from m_Z, the cross-section is dominated by electromagnetic interaction (mediated by γ). The reaction $e^+e^- \rightarrow \gamma \rightarrow f\bar{f}$ is in the Born approximation described by the matrix element [59]:

$$\mathcal{M}_\gamma = -q^f q^e \left[\bar{f}\gamma^\nu f\right] \left(\frac{\mathrm{g}_{\nu\mu}}{k^2}\right) \left[\bar{e}\gamma^\mu e\right] \tag{0.6}$$

where f and e are the fermion fields, q^f and q^e their charges and k^2 is the four-momentum squared carried by the mediating photon. γ^ν, γ^μ denote standard 4×4 gamma matrices and $\mathrm{g}_{\nu\mu}$ is a totally antisymmetric tensor. Here no polarization is generated since the vertices contain only parity conserving **V** coupling. Precisely, emerging fermions are unpolarized in case of unpolarized e^+ and e^- beams which is the case of LEP. The electromagnetic cross-section drops as $1/\mathbf{s}$ where $\mathbf{s}{=}E^2_{\mathrm{CM}}$. In contrast, the weak interaction mediated by the massive Z^0 has a resonant character. In the Born approximation it is governed by the matrix element [59]:

$$\mathcal{M}_Z = -\frac{g^2}{4\cos^2\Theta_W} \left[\bar{f}\gamma^\nu(c^f_{\mathrm{V}} - c^f_{\mathrm{A}}\gamma^5)f\right] \left(\frac{\mathrm{g}_{\nu\mu} - \dfrac{k_\nu k_\mu}{m^2_Z}}{k^2 - m^2_Z}\right) \left[\bar{e}\gamma^\mu(c^e_{\mathrm{V}} - c^e_{\mathrm{A}}\gamma^5)e\right] \tag{0.7}$$

where apart from already defined symbols we have: $k_{\nu,\mu}$ denoting four-momentum transferred by the Z^0, weak coupling constant g and the Z^0 mass m_Z. The vertices being linear combinations of **V** and **A** couplings lead to a fractional parity violation and fermions produced in the Z^0 decay obtain a non-zero longitudinal polarization. Its value depends on vector and axial-vector couplings of the electron and the given fermion to the Z^0 boson as will be shown in the following section.

At E_{CM} close to the Z^0 mass the weak neutral interaction completely predominates over the electromagnetic contribution. The total cross-section of the $e^+e^- \rightarrow Z^0(\gamma) \rightarrow f\bar{f}$ is shown in Fig. 6. Around the Z^0 resonance the cross-section is dominated by the weak neutral boson exchange by almost three orders of magnitude. Therefore, when discussing the properties of fermions produced at LEP1 we can make a good approximation that the e^+e^- annihilation is saturated by Z^0 production.

From equation (0.7) in the limit of negligible fermion masses and for unpolarized e^+ and e^- beams one may derive the fundamental electroweak predictions for LEP1 physics:

- Z^0 branching fractions:

$$\mathrm{BR}(Z^0 \longrightarrow f\bar{f}) = \frac{(c^f_{\mathrm{V}})^2 + (c^f_{\mathrm{A}})^2}{\sum_i \left((c^i_{\mathrm{V}})^2 + (c^i_{\mathrm{A}})^2\right)} \tag{0.8}$$

[1] As was already mentioned in the introduction the SLAC linear collider has comparable sensitivity to most of the electroweak parameters. However, typically they are accessed via different physics processes due to the polarized e^+e^- beams.

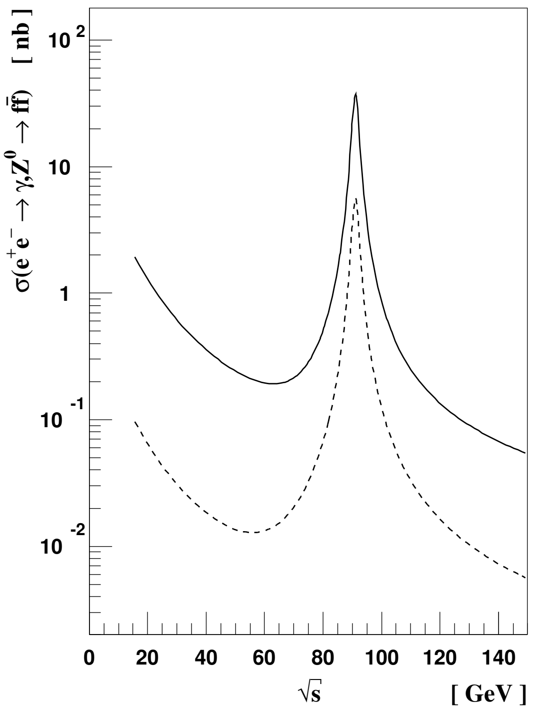

Figure 6: The effective cross-section for the process $e^+e^- \to Z^0(\gamma) \to f\bar{f}$ as a function of the center-of-mass energy $\sqrt{\mathrm{s}}$. The solid line represents the total cross-section containing contributions from l^+l^-, $\nu\bar{\nu}$ and $q\bar{q}$ in the final state. The dashed line gives the partial cross-section leading to a $b\bar{b}$ pair only.

- forward-backward asymmetry:

$$\mathrm{A_{FB}} = \frac{\Gamma_\mathrm{F} - \Gamma_\mathrm{B}}{\Gamma_\mathrm{F} + \Gamma_\mathrm{B}} = \frac{3}{4}\mathcal{A}_e\mathcal{A}_f \tag{0.9}$$

  where $\mathcal{A} = \dfrac{2c_\mathrm{V}c_\mathrm{A}}{c_\mathrm{V}^2 + c_\mathrm{A}^2}$; Γ_F and Γ_B represent the probabilities of finding a final-state fermion in the incoming e^+ beam hemisphere and the incoming e^- beam hemisphere respectively.

- mean fermion longitudinal polarization:

$$\langle P_f \rangle = -\mathcal{A}_f \tag{0.10}$$

The latter one is of fundamental interest to our analysis and thus will be discussed separately in more detail in the following section.

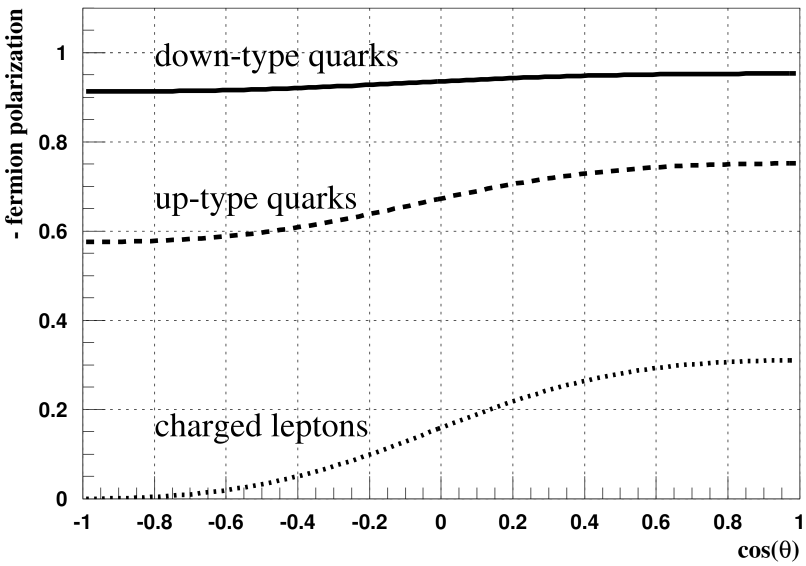

Figure 7: Standard Model prediction for the longitudinal polarization of fermions produced in $e^+e^- \to Z^0 \to f\bar{f}$ as a function of the production angle θ.

3.1 Polarization of fermions from $e^+e^- \to Z^0 \to f\bar{f}$

The polarization of fermions produced in the reaction $e^+e^- \to Z^0 \to f\bar{f}$ is precisely predicted in the framework of the Standard Model. In the case of unpolarized e^+e^- beams the formula for longitudinal polarization as a function of the fermion production angle θ reads [60]:

$$P_f = -\frac{\mathcal{A}_f(1+\cos^2\theta) + 2\mathcal{A}_e\cos\theta}{1+\cos^2\theta + 2\mathcal{A}_e\mathcal{A}_f\cos\theta} \qquad \text{where} \quad \mathcal{A} = \frac{2c_V c_A}{c_V^2 + c_A^2} \tag{0.11}$$

Here θ is the angle between the emerging fermion f and the e^- beam in the center of mass reference frame. c_V and c_A denote the vector and axial-vector couplings of the fermion to the Z^0 boson. The formula is exact in the limit of negligible fermion masses ($m_f/m_{Z^0} \to 0$). Charged fermion polarization plotted as a function of the production angle θ is shown in Fig. 7. The absolute magnitude of the polarization is identical for f and $\bar{f}$ while the sign is opposite ($\bar{f}$ have positive polarization). Having integrated over the θ angle we are left with the mean fermion polarization:

$$\begin{aligned} \langle P_{e,\mu,\tau}\rangle &= -\mathcal{A}_e \cong -0.16 \\ \langle P_{u,c}\rangle &= -\mathcal{A}_u \cong -0.66 \qquad\qquad \text{assuming} \quad \sin^2\Theta_W = 0.23 \\ \langle P_{d,s,b}\rangle &= -\mathcal{A}_d \cong -0.94 \end{aligned} \tag{0.12}$$

Clearly, the down-type quarks (and b among them) are most strongly polarized. Their absolute polarization is close to unity. Moreover, it is fairly stable over the whole range of the production angle. Neither gluon nor photon radiation from the final state are predicted to degrade this high polarization [61, 62]. The first possibility of altering the primary b quark spin state arises during (and after) hadronization.

Only the polarization of the τ lepton is directly experimentally accessible. It has been already widely explored by the LEP experiments [63, 64, 65, 66]. Electrons are stable and muons live much too long to decay inside the detector ($c\tau_\mu = 659$ m [19]). Hence there is no way to analyze their polarization. Quarks in turn always hadronize before they decay and this process usually changes their spin state. However, this does not always have to be the case. In the following section we will present theoretical predictions concerning this matter.

3.2 b quark hadronization in the HQET approximation

The **H**eavy **Q**uark **E**ffective **T**heory (HQET) [67, 68, 69] is now the most popular tool to describe properties of hadrons containing a single heavy quark Q bound with a light quark (or diquark). The approach is based on the large heavy quark mass limit $m_Q \to \infty$. This limit is applicable for $m_Q \gg \Lambda_{\mathrm{QCD}}$ which is well satisfied in the case of the b quark. In the HQET approximation the light quark degrees of freedom become insensitive to the mass m_Q. In particular a new "heavy quark spin-flavour symmetry" emerges which eliminates the hyperfine spin interaction between the heavy quark and the light component.

A single quark emerging from the e^+e^- interaction point carries the strong interaction charge – colour. Because of the confinement it cannot exist alone away from a twin antiquark at a distance bigger than the strong interaction range (typically ≈ 1Å). To cross this barrier a free quark has to undergo the hadronization process and form a colour singlet. Hadronization can be interpreted as a dressing of a free primary quark carrying a colour charge with a light antiquark or a diquark to form a colourless bound state – hadron. In about 90% of the cases the primary quark picks a single antiquark from the spontaneously produced $q\bar{q}$ pair and forms a meson. Hadronization to baryons accounts only for about one tenth of the total rate.

During hadronization to mesons the information about the heavy quark spin state is lost. The heavy b quark couples with a light antiquark having the same or opposite orientation of the spin projection with an equal probability[1]:

$$|\uparrow\rangle_b|\uparrow\rangle_{\bar{q}} \qquad \text{or} \qquad |\uparrow\rangle_b|\downarrow\rangle_{\bar{q}} \tag{0.13}$$

In the first case some of the initial b polarization may be retained but such an excited

[1]see ref. [70] for explicit wavefunctions, etc.

state would subsequently decay radiatively to a spin-0 B meson in a much shorter time scale than the slow weak decay of the b quark. The second state (0.13) is in reality a linear combination of a $\bar{B}$ and a $\bar{B}^*$ meson since the mass and spin meson eigenstates are not identical [71, 72]. Because of the B–B^* mass splitting the two components propagate incoherently and again the b quark spin information is lost before the meson can decay due to a weak interaction.

However, in case of hadronization to a ground baryonic state the complete transfer of the b polarization to a Λ_b baryon makes an important prediction of the Heavy Quark Effective Theory. In the HQET approximation the spin degrees of freedom of a heavy quark are decoupled from a spin-zero light diquark:

$$|\uparrow\rangle_b|\mathrm{S}=0\rangle_{qq} \tag{0.14}$$

Therefore in the heavy quark limit a b quark hadronizing directly to a Λ_b should pass its complete initial polarization to the baryon and then conserve it throughout the whole Λ_b lifetime.

3.3 Possible depolarization effects

In real life however, a large fraction of Λ_b's can be produced indirectly through the heavier Σ_b and Σ_b^* states:

$$\begin{array}{c} b \longrightarrow \Sigma_b \longrightarrow \Lambda_b^0 + \pi \\ b \longrightarrow \Sigma_b^* \longrightarrow \Lambda_b^0 + \pi \end{array} \tag{0.15}$$

Processes (0.15) are predicted to lead to a substantial depolarization of the heavy quark. A detailed discussion of different scenarios of the indirect hadronization is given in [72, 73].

Heavier states $\Sigma_b^{(*)}$ are created when a b quark combines with a diquark carrying spin S=1. As a result baryons with total spin S=$\frac{1}{2}$(Σ_b) or S=$\frac{3}{2}$(Σ_b^*) are produced:

$$|\uparrow\rangle_b|\downarrow\downarrow\rangle_{qq} \qquad \text{or} \qquad |\uparrow\rangle_b|\uparrow\uparrow\rangle_{qq} \tag{0.16}$$

Predicting for the fraction of $\Sigma_b^{(*)}$ in the total b-baryon production is difficult and depends on the model. Reference [72] gives a value of 30% as a reasonable approximation. In contrast, the relative production rate derived from the spin counting is Σ_b:Σ_b^* =1:2 and is independent from the modeling. Motivated by the c sector spectroscopy it is assumed that $\Sigma_b^{(*)}$ states lie over 140MeV above the Λ_b and can decay via processes (0.16). It is argued in [72] that the final polarization of Λ_b's from (0.16) depends on the

$\Sigma_b^{(*)}$ resonance character Γ/Δ as well as on the diquark spin alignment parameter w_1. Γ is the total width of $\Sigma_b^{(*)}$ states and Δ is the Σ_b–Σ_b^* mass splitting. The w_1 parameter is the probability that the spin 1 diquark ($\Sigma_b^{(*)}$ constituent) has a maximum angular momentum $j^3 = \pm 1$ along the fragmentation axis. In the extreme case of $\Gamma/\Delta \ll 1$ and $w_1 = 0$, Λ_b's from the Σ_b^* cascade are predicted to retain only $\frac{1}{3}$ of the initial b polarization while the Σ_b cascade retains the same absolute value of the polarization but inverts its sign (-$\frac{1}{3}$)! However, in the case of very wide $\Sigma_b^{(*)}$ resonances ($\Gamma/\Delta \gg 1$) complete conservation of the primary polarization is predicted independently from w_1.

The first evidence for the $\Sigma_b^{\pm}$ and $\Sigma_b^{*\pm}$ production at LEP has already been reported by the DELPHI experiment [52]. According to the measurement $\Sigma_b^{\pm}$ and $\Sigma_b^{*\pm}$ appear to be distinct narrow resonances ($\Gamma/\Delta \ll 1$) and are indeed heavy enough to decay via processes (0.16). $\Sigma_b^{(*)}$'s are estimated to account for roughly half of the initial b baryon states. The result indicates a high contribution of the excited states, although one should bear in mind its big error of 30% . Combining the experimental results with the theoretical arguments given above one expects that the inclusive Λ_b sample should retain at least (63% $\pm$ 18)% of the initial quark polarization. The limit value corresponds to $w_1 = 0$. From this, multiplying by the initial b polarization $P_b = -0.94$ we obtain a prediction for the effective Λ_b polarization $P_{\text{effective}} \geq -0.59 \pm 0.17$.

Summarizing, we have shown here that the Λ_b polarization measurement should give vital information about the b quark hadronization into heavy baryons and constitutes a subsequent test of the HQET as well as of the SM prediction for the polarization of the primary $b\bar{b}$ quarks.

3.4 SM description of the semileptonic decay $\Lambda_b^0 \to \Lambda_c^+ l\bar{\nu}$

In the Born approximation of the free quark the differential rate of the decay $b \to c + l + \bar{\nu}$ is proportional to a simple matrix element [74]:

$$d\Gamma^{(0)} \sim |\mathcal{M}^{(0)}|^2 d\mathbf{R}_3 \tag{0.17}$$

where

$$|\mathcal{M}^{(0)}|^2 = (\mathbf{cl})\,((\mathbf{b} - m_{\mathrm{b}}\mathbf{S}_{\mathrm{b}})\boldsymbol{\nu}) \tag{0.18}$$

b,**c**,**l** and $\boldsymbol{\nu}$ denote four-momenta of the involved fermions and $\mathbf{S}_{\mathrm{b}}$ is the b quark spin four-vector. The spin dependence of the matrix element comes from the maximally parity violating character of the **V-A** current attributed to the $W^{\pm}$ exchange. In the rest frame of the b quark $\mathbf{S}_{\mathrm{b}}$ has the form $\begin{pmatrix} 0 \\ \vec{s} \end{pmatrix}$. Hence the matrix element exhibits a nice factorization of the spin direction component [75]:

$$|\mathcal{M}^{(0)}|^2 = |\mathcal{M}^{(0)}_{\text{unpol}}|^2\,(1 + P\cos\theta) \tag{0.19}$$

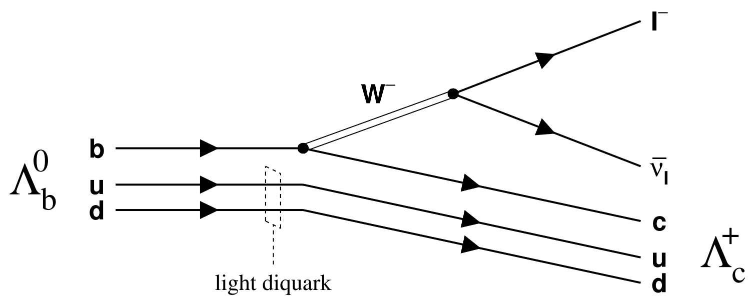

Figure 8: The Born level graph of the Λ_b semileptonic decay in the HQET approximation.

where θ is the angle between the neutrino momentum and the spin quantization axis (see Fig. 3).

The formula for the double-differential distribution (θ angle and energy y) of the b decay products (charged and neutral leptons) reads [62]:

$$\frac{d^2\Gamma}{dy\, d\cos\theta} = \frac{d\Gamma}{dy}\frac{1}{2}[1 + P\alpha(y)\cos\theta] \tag{0.20}$$

$$\alpha_l(y) = \frac{(1-2y)(1-y) - \epsilon(1+y)}{(3-2y)(1-y) + \epsilon(3-y)} \qquad \alpha_\nu(y) = 1$$

$$\text{where} \quad y = \frac{2E}{m_b} \quad \text{and} \quad \epsilon = \frac{m_c^2}{m_b^2}$$

Here E is the decay product energy in the b rest frame while m_b and m_c denote free b and c quark masses. P is the b quark polarization. The formula (0.20) is derived in the limit of vanishing lepton mass ($m_l/m_b \to 0$). For the neutrino we have the factorization of the angular dependent term since $\alpha_\nu(y) \equiv 1$. However, this is not the case for the charged lepton. The α coefficients for charged lepton and neutrino as a function of the fractional energy y are shown in Fig. 9. They reflect directly the sensitivity to the b polarization. The angular asymmetry factor α for charged leptons is smaller than 1 and even changes its sign for small y. In contrast neutrino angular asymmetry is identically equal to unity and thus reflects the original polarization of the bottom quark without any loss of information.

So far we have discussed only the 0-order approximation described by the matrix element $|\mathcal{M}^{(0)}|$. The natural question arises to what extent the higher order corrections

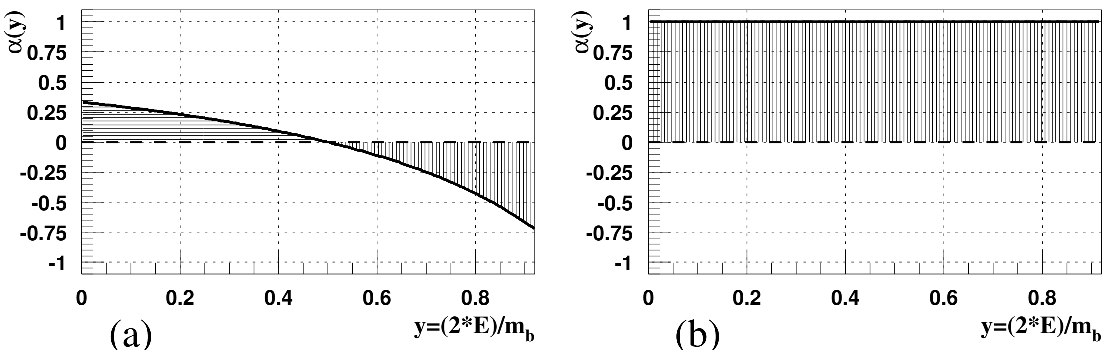

Figure 9: The forward-backward asymmetry coefficients α for the polarized b quark decay; (a) charged leptons (e or μ), (b) neutrinos (ν_e or ν_μ).

distort this simple picture. First order QCD corrections for the process (0.18) have been calculated [74, 75, 76]. A virtual gluon exchange and a real gluon emission contribute to the total matrix element $|\mathcal{M}|^2 = |\mathcal{M}^{(0)}|^2 + |\mathcal{M}^{\mathrm{exchange}}|^2 + |\mathcal{M}^{\mathrm{emission}}|^2$. A priori the correction terms do not retain the straightforward factorization (0.19) but fortunately even in this case the angular dependent and independent parts cancel to a large extent in the ratio. In practice factorization is violated only at the level of one percent and hence having absorbed all corrections to the overall normalization we can assume that

$$|\mathcal{M}|^2 \cong |\mathcal{M}_{\mathrm{unpol}}|^2 \,(1 + P\cos\theta) \tag{0.21}$$

Furthermore, it should be stressed that the calculated QCD corrections are very small when compared with the present experimental accuracies. As such they have been considered negligible and are not taken into account in the following analysis. In particular the Λ_b polarization in the Monte Carlo simulation will be generated using the approximation (0.21).

It can be argued that when going to real heavy baryon decays the dynamics of the reaction $\Lambda_b^0 \to \Lambda_c^+ l + \nu$ (Fig. 8) remains identical with the free quark case discussed above [69]. This approximation is derived from the leading order of the Heavy Quark Effective Theory which has already confirmed its predictive power in b hadron spectroscopy [67].

As already mentioned the $\bar{b}$ quarks are born with opposite longitudinal polarization to the b quarks. However from the CP invariance of the weak decay $\Lambda_b^0 \to \Lambda_c^+ l + \nu$ the final differential distributions of the charged lepton and neutrino look the same after the charge conjugate operation. Consequently, both Λ_b and $\bar{\Lambda}_b^0$ semileptonic decays lead to the same momentum distributions of the decay products.

4 Experimental approach to the Λ_b polarization measurement (possibilities and limitations)

In this chapter we will briefly summarize the phenomenological assumptions used in the presented analysis. The choice of the Λ_b decay channel as well as the observable used to determine its polarization will be introduced. Throughout this paper by charged lepton we refer to either electron or muon. In all discussions charge conjugate reactions are implied.

4.1 Choice of the decay channel

In the analysis presented here the Λ_b polarization is studied in its semileptonic decay channels with a Λ^0 reconstructed in the final state. The Λ_b cascade decay can be written as:

$$\begin{array}{l} \Lambda_b^0 \to X_c + l^- + \bar{\nu}_l \\ X_c \to \Lambda^0 + X \\ \Lambda^0 \to p + \pi^- \end{array} \tag{0.22}$$

Here X_c denotes any charmed baryon and the letter l stands for a charged lepton. There are several reasons for choosing this channel.

First of all, it has a fairly high branching fraction. Although the Λ_b semileptonic branching fractions have not been directly measured we make an approximate assumption that they are close to the B meson ones [19]:

$$\begin{array}{rcl} \mathrm{BR}(B \longrightarrow e^+\nu_e \mathrm{anything}) & = & (10.4 \pm 0.4)\% \\ \mathrm{BR}(B \longrightarrow \mu^+\nu_\mu \mathrm{anything}) & = & (10.3 \pm 0.5)\% \end{array} \tag{0.23}$$

Hence we expect the two semileptonic branching fractions to contribute to some 20% of the total Λ_b decay rate. Motivated by the b-meson sector we may expect that the c baryon X_c in formula (0.22) should nearly always be the Λ_c particle [69]. Similarly as reactions $B \to Dl\nu$ and $B \to D^*l\nu$ saturate the inclusive rate of $B \to X_cl\nu$ the semileptonic decays of Λ_b should be almost saturated by $\Lambda_b \to \Lambda_cl\nu$, namely to about 90%. Λ_b can also decay to $\Sigma_cl\nu$ (with a subsequent Σ_c decay into $\Lambda_c\pi$) but such transitions are suppressed by at least one power of Λ_{QCD}/m_c [69]. The inclusive branching fraction of Λ_c to Λ^0+anything is known to be $(35 \pm 11)\%$ [19]. Combining the above two pieces of information we get an estimate of the branching fraction for the cascade (0.22) to be $\approx$7%.

Secondly there is a relatively easy way of tagging the Λ_b through Λ^0 lepton correlations [24, 45]. These decays have the following properties: the lepton is highly energetic and has high transverse momentum[1] relative to the jet axis and the Λ^0 has a harder momentum spectrum than the Λ^0 baryons produced from the fragmentation see. Moreover, $\Lambda^0 l$ pairs originating from a b baryon cascade have a well defined correlation between the lepton charge and the Λ^0 baryonic number. For brevity it will be called charge correlation. The b baryon signal is uniquely related to $\Lambda^0 l^-$ (or $\bar{\Lambda}^0 l^+$) correlations, hereafter called *right-sign* (R.S.). $\Lambda^0 l^+$ (or $\bar{\Lambda}^0 l^-$) correlations, hereafter called *wrong-sign* (W.S.), have a purely background origin. As will be shown in section 5.3, practically all background events have no physically preferred charge correlation and therefore are equally distributed among the two classes. Hence, the excess of *right-sign* events over *wrong-sign* ones is attributed to the semileptonic decays of the Λ_b baryon.

Finally, there are precise Standard Model predictions for the dynamics of the polarized Λ_b semileptonic decay. These were widely discussed in section 3.4.

Similarly, semileptonic decays of the Λ_b can be also tagged through the pl correlations where the proton comes from the Λ_c decay or in a more exclusive way via the $\Lambda_c l$ correlations where Λ_c is fully reconstructed in its hadronic decay [77]. Both methods were proposed and recently developed for the benefit of the Λ_b lifetime measurement. The first one strongly relies on the good performance of the DELPHI RICH detectors and has become experimentally feasible only recently. The latter one relies on the good charged track reconstruction and uses RICH identification power to reduce combinatorial background. Unfortunately it is still statistically limited and hence cannot serve as a valuable input for the polarization measurement.

An alternative approach would be to use the more numerous hadronic Λ_b decays. Apparently, however, they create immense difficulties in the experimental reconstruction. Searches for exclusive hadronic decays typically end up with a few event candidates and can be used at most for the precise mass determination [25]. Besides, all hadronic decay modes inevitably involve QCD dynamics in the nonperturbative region of low energies and cannot give precise enough theoretical predictions.

4.2 Observables

Hereafter we will refer only to the semileptonic Λ_b decays with a Λ^0 in the final state as justified in the previous section.

The best way to measure the polarization would be to look at the forward-backward

[1] The maximal possible transverse momentum $p_T^{\max}$ is strongly related to the mass of the decaying object M. The limit is defined by the formula: $p_T^{\max} = \frac{1}{2}\sqrt{M^2 - m_{eff}^2}$, where $m_{eff}^2 = \sum_i m_i^2$ and the summing is over all decay products. Hence, the decays of the heavy particles are characterized by the high p_T of their decay products. Clearly, the above p_T is defined relative to the heavy b-hadron momentum direction. At LEP this reference axis is satisfactorily reproduced by the direction of the reconstructed jet containing the b-hadron.

asymmetries of Λ_b decay products in its rest frame. These observables are directly related to polarization. However, as discussed above we are not able to fully reconstruct the Λ_b four-momentum. With the available event statistics we can only aim to reconstruct the Λ_b in the semi-inclusive channels. Besides in the semileptonic decay mode the escaping neutrino makes the precise Λ_b momentum reconstruction impossible anyway.

Experimentally we are effectively limited to the laboratory frame observables. Fortunately Λ_b baryons produced in Z^0 decays are highly boosted in the laboratory frame. In such a case the forward-backward asymmetry of the decay product can be directly expressed in terms of a shift in the average value of its energy spectrum in the laboratory frame. The rapidity y is defined as:

$$y = \frac{1}{2}\ln\left(\frac{E+p_{||}}{E-p_{||}}\right) \equiv \ln\left(\frac{E+p_{||}}{m_{\perp}}\right) \qquad \text{where} \qquad m_{\perp}^2 = m^2 + p_{\perp}^2 \tag{0.24}$$

Rapidity transforms additively with the Lorenz boost ($y \xrightarrow{boost} y' = y + \mathrm{arth}\beta$). Hence $E + p_{||}$ transforms multiplicatively:

$$(E+p_{||})' = \exp^{\Delta y}(E+p_{||}) = (1+\beta)\gamma(E+p_{||}) \tag{0.25}$$

hence

$$\langle E+p_{||}\rangle_{\mathrm{LAB}} = \langle(1+\beta)\gamma\rangle\langle E+p_{||}\rangle_{\Lambda_b\mathrm{rest}} \tag{0.26}$$

The latter comes from the independence of the boost (fragmentation function) and the Λ_b decay kinematics.

There have been several theoretical proposals to probe the Λ_b polarization using only an average charged lepton energy in the laboratory frame [60, 69, 71]. This method has two considerable disadvantages making it unrealistic. First the charged lepton shows too little sensitivity to the Λ_b polarization and secondly and even more important, it is experimentally impossible to disentangle the a priori unknown Λ_b fragmentation function from the reconstructed lepton spectrum. In other words, there is no good unpolarized reference to compare to. Some authors [60, 62] have proposed using B meson semileptonic decays at LEP as an unpolarized reference or to look at the lower energy e^+e^- machines (like PETRA at DESY) where the lack of polarization is guaranteed by the electromagnetic character of the reaction $e^+e^- \rightarrow \gamma \rightarrow q\bar{q}$. Unfortunately in both cases theoretical uncertainties on the b fragmentation are of the same order as the lepton spectrum variations induced by the polarization.

Considering both the charged lepton and the neutrino from semileptonic Λ_b decays as the polarization probe turns out to be far more promising approach, which eventually

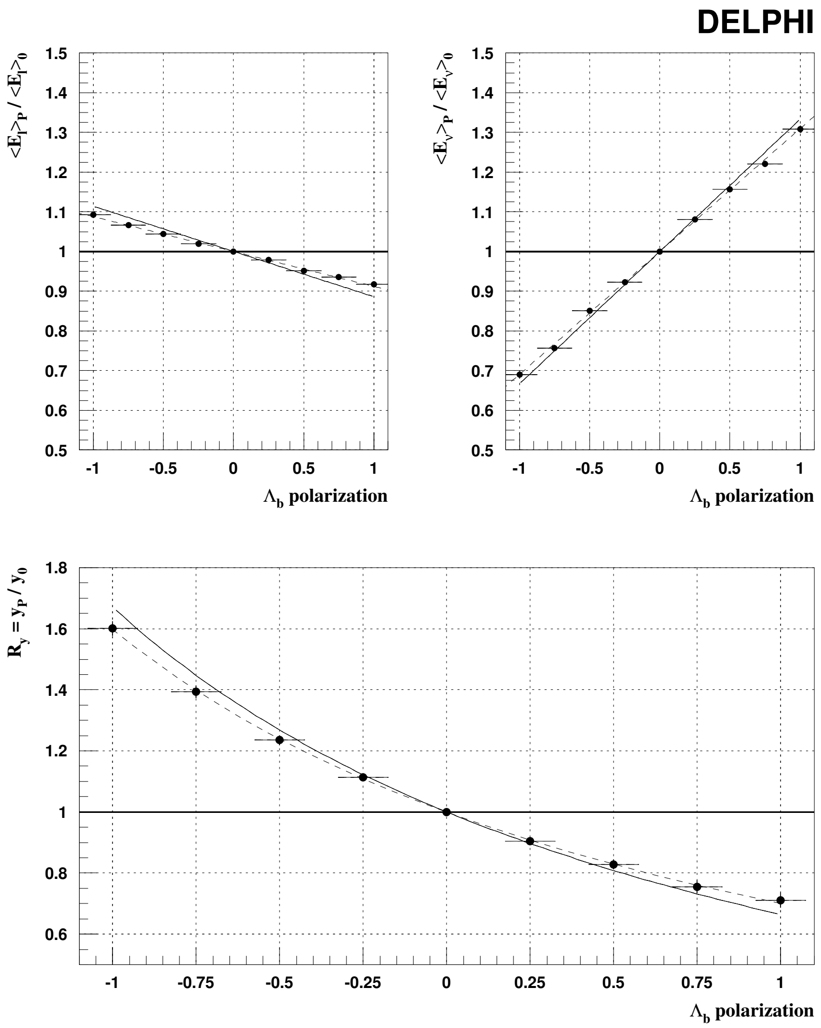

Figure 10: Theoretical dependence of $\langle E_l \rangle / \langle E_l \rangle_{P=0}$, $\langle E_\nu \rangle / \langle E_\nu \rangle_{P=0}$ and R_y on the Λ_b^0 polarization (m_b=5GeV/c^2, m_c=1.4GeV/c^2). The overlaid Monte Carlo points represent the actual experimental sensitivity after the whole analysis procedure. The dashed line is a fit to the Monte Carlo response. For details on simulation of polarized Λ_b decays see section 4.3.

makes the measurement of Λ_b polarization feasible. As was shown in the previous chapter, the neutrino is the decay product most sensitive to the Λ_b polarization [74, 75]. Indeed, the charged lepton is over three times less sensitive. The upper plots in Fig. 10 show the dependence of $\langle E_l \rangle / \langle E_l \rangle_{P=0}$ and $\langle E_\nu \rangle / \langle E_\nu \rangle_{P=0}$ on the Λ_b polarization as predicted by the Standard Model and the HQET. From the plots in Fig. 10 one can see that the average energies of the charged lepton and the neutrino are respectively

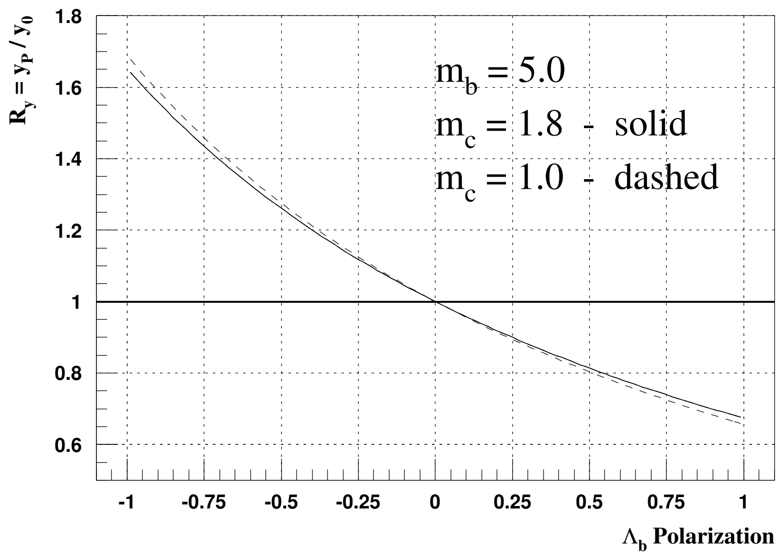

Figure 11: Theoretical dependence of R_y as a function of Λ_b^0 polarization for two extreme m_c^2/m_b^2 choices.

anti-correlated and correlated with the polarization. Hence, the variable defined as:

$$y = \frac{\langle E_l \rangle}{\langle E_\nu \rangle} \tag{0.27}$$

turns out to be highly sensitive to Λ_b polarization [78]. Moreover, this observable is explicitly independent of fragmentation uncertainties. We have:

$$\frac{\langle E \rangle_l^{\mathrm{LAB}}}{\langle E \rangle_\nu^{\mathrm{LAB}}} \cong \frac{\langle E + p_{||} \rangle_l^{\mathrm{LAB}}}{\langle E + p_{||} \rangle_\nu^{\mathrm{LAB}}} \equiv \frac{\langle E + p_{||} \rangle_l^{\Lambda_b \mathrm{rest}}}{\langle E + p_{||} \rangle_\nu^{\Lambda_b \mathrm{rest}}} \tag{0.28}$$

Here $p_{||}$ is the particle momentum projection on the Λ_b direction of flight. The left equality is perfectly satisfied in the LEP environment where for leptons $p_{||}^{\mathrm{LAB}} = E^{\mathrm{LAB}}$ to a percent level. The right equality is exact and comes from the explicit Lorentz invariance of the right hand quantity (see formula 0.26). This crucial observation allows one to overcome the substantial problem of Λ_b energy reconstruction.

In reality the observed energy spectra undergo several deformations because of detector response and selection cuts. To correct for these effects the variable y obtained from the data has been normalized to the one extracted from an explicitly unpolarized Monte Carlo. Therefore, the final observable is defined:

$$R_y = \frac{y^{\mathrm{DATA}}}{y^{\mathrm{MC}}} \tag{0.29}$$

The overlaid Monte Carlo points in Fig. 10 show the actual experimental response to the Λ_b polarization after the entire analysis which will be described in section 5. Details of the simulation of polarized Λ_b decays will be given in section 4.3. As can be seen, the analysis cuts and the detector inefficiencies introduce a certain loss of sensitivity in particular in the charged lepton sector. However, the attenuation of the sensitivity is small (around 10%) and the final R_y curve fitted to the Monte Carlo points still preserves high sensitivity to the polarization. It should be noted, that the curve resulting from a fit to the R_y points reconstructed in simulation is of a fundamental importance to this analysis. It will be used to extract the polarization of Λ_b after determining the value of R_y from data.

Fig. 11 shows the theoretical dependence of $y/y_{P=0}$ (where y is normalized to the unpolarized case) as a function of the Λ_b polarization. Here the only theoretical uncertainty comes from the unknown quark masses m_c and m_b. In practice they enter to the calculations as a single parameter m_c^2/m_b^2. As seen from Fig. 11 y is fortunately very weakly sensitive to quark masses. However, this possible variation will be accounted for in the systematic error.

The proposed approach requires a reasonable knowledge of the escaping neutrino energy E_ν. In the LEP environment such a determination is achievable using the hemisphere missing energy method described in detail in section 5.5. As will be argued, the hemisphere energy determination is well reproduced by the simulation. Therefore, any deviation of R_y from unity observed in the background subtracted Λ_b signal sample will be attributed to the Λ_b polarization.

4.3 Polarized Λ_b decays in the simulation

The JETSET program [79] by its construction does not retain any information about the spin of the partons and hence of the produced hadrons. In particular, the semileptonic decay of the Λ_b baryon is simulated as if the Λ_b was unpolarized. This means that the decay follows the matrix element $\mathcal{M}_{\mathrm{unpol}}$ and since there is no distinguished direction the single-particle angular distribution of any decay product has a spherical symmetry.

In the presence of polarization the latter is no longer true. The spin quantization axis (direction w.r.t. which we define polarization) is now well defined. In case of Λ_b this axis points along the Λ_b boost direction. As is argued in section 3.4, in the Λ_b

semileptonic decay a special role is played by the angle θ between the spin quantization axis and the direction of the momentum of the neutrino in the Λ_b rest frame.

To simulate semileptonic decays of polarized Λ_b it is sufficient to scale the rate of unpolarized decays by the factor $(1 + P\cos\theta)$ as given in formula 0.21. Therefore, in order to mimic the polarization we perform the Monte Carlo rejection:

$$\texttt{if (} (1 + |P|)x_{\texttt{rnd}} > (1 + P\texttt{cos}\theta) \texttt{) skip the event} \tag{0.30}$$

where P is the Λ_b polarization and $x_{\texttt{rnd}}$ is a random number from a flat distribution ranging from zero to one.

The described procedure is exact at the Born level and still makes a sufficiently good approximation after including QCD corrections as argued in the previous chapter.

5 Analysis procedure

This chapter describes in detail all experimental aspects of the presented analysis. First the general event requirements together with the signal selection are comprehensively described. Then we discuss the background composition and the method of its subtraction. Finally we give an extensive account of the neutrino energy reconstruction algorithm. This chapter also contains a brief description of the selection of the auxiliary B meson signal used as a consistency check of the results obtained for the Λ_b baryon.

The analysis is based on $\approx 3\times 10^6$ hadronic Z^0 decays collected by the DELPHI detector in the 1993 to 1995 data-taking periods.

To evaluate the reference y^{MC} (see formulae (0.27) and (0.29)) we use a sample of 45,000 background free $b \to \Lambda_b^0$ Monte Carlo events processed through the full simulation of the DELPHI apparatus. From this sample over 2,000 candidates for the cascade decay $\Lambda_b^0 \to l\nu\Lambda^0 X$ remain after the whole reconstruction and the complete analysis selection. In this analysis background events give the main contribution to the statistical error. Therefore, in the highly populated background free sample the reference y^{MC} for the genuine Λ_b signal is determined with a very high statistical sensitivity. As a result the statistical error on the extracted R_y induced by the MC reference (y^{MC}) has been reduced to an almost negligible level.

To cross-check our signal selection and result extraction we use an unbiased sample of over 4 million Monte Carlo hadronic Z^0 events which have also been processed through the full simulation of the DELPHI apparatus. In this sample about 450 Λ_b signal events have been reconstructed. This Λ_b population is only five times smaller than the one obtained from the dedicated Monte Carlo discussed above. However, since here the signal is not background free it follows that the value of y^{MC} is extracted with a considerable error. Hence, this sample is not used as our MC reference. It serves only as an independent consistency check of the analysis.

The above two Monte Carlo samples are fully independent.

---

[1]The quantity thrust T is defined as: $T = \max\limits_{|\mathbf{n}|=1} \frac{\sum_i |\boldsymbol{n}\cdot\boldsymbol{p_i}|}{\sum_i |\boldsymbol{p_i}|}$, where the sum goes over all particles reconstructed in the event. $\boldsymbol{p}$ denotes the particle three-momentum and $\boldsymbol{n}$ is a unit-length space vector. The thrust axis is given by the $\boldsymbol{n}$ for which a maximum is attained. The allowed range is $1/2 \leq T \leq 1$, with a 2-jet event corresponding to $T \approx 1$ and an isotropic event to $T \approx 1/2$.

5.1 Global event selection

As a first step events are required to satisfy the standard DELPHI selection of hadronic events [54]. The hadronic event selection in DELPHI is meant to guarantee a high and a well understood efficiency. Hadronic Z^0 decays are selected as events with a multiplicity above 4 of charged particles with $p > 0.4$ GeV/c, $20° < \theta < 160°$ and a track length of at least 30 cm in the TPC, with a total energy carried by these particles of above $0.12 \times E_{\rm cm}$. Additionally the calculated thrust axis[1] has to satisfy a condition $|\cos\theta_{\rm thrust}| < 0.95$. The efficiency of such an event selection is over 95%. The background, mainly from $\tau^+\tau^-$ pairs with smaller contribution of $\gamma\gamma$ collisions, is below 0.7%.

Next, events are subdivided into two hemispheres by a plane perpendicular to the thrust axis and containing the interaction point (Fig. 12). A tighter cut on the thrust axis direction is applied. Each event is required to have $\mid \cos(\theta_{thrust}) \mid < 0.866$ which corresponds to the θ range (30°;150°). For the missing energy measurement it is essential to have events well contained in the detector fiducial volume where the reconstruction efficiency is high and relatively well controlled. In order to suppress events with hard gluon radiation the calculated thrust value is required to exceed 0.75. More isotropic events are likely to contain three or more energetic jets and hence tend to spoil the hemisphere energy evaluation. Moreover the total visible energy reconstructed in an event has to be between 30 GeV and 130 GeV. This cut rejects a very small fraction of events where the total energy is abnormally badly measured due to a large noise cluster in the calorimeter or totally screwed momentum assigned to a charged track (tracking imperfection).

5.2 Λ_b signal selection

As discussed in section 4.1, events with a high p_T charged lepton and a Λ^0 in the final state contribute to the Λ_b signal.

Selection of leptons from the b quark decay

Lepton candidates (electrons or muons) are selected requiring a "standard tag" according to the identification algorithms described in chapter 2.2. Furthermore, they have to satisfy the so called "good track" requirements; track length > 30 cm, error on momentum < 25%, $R\phi_{\rm impact\ parameter} < 4$ cm and $Rz_{\rm impact\ parameter} < 10$ cm. To this preselected lepton sample two main kinematical cuts are applied:

- $p(l) > 3.0$ GeV/c – below 3 GeV/c the performance of the lepton identification degrades significantly,
- $p_T^{out}(l) > 0.8$ GeV/c – this enriches the sample in leptons from semileptonic b decays as argued in section 4.1; the superscript *out* means that the jet is defined

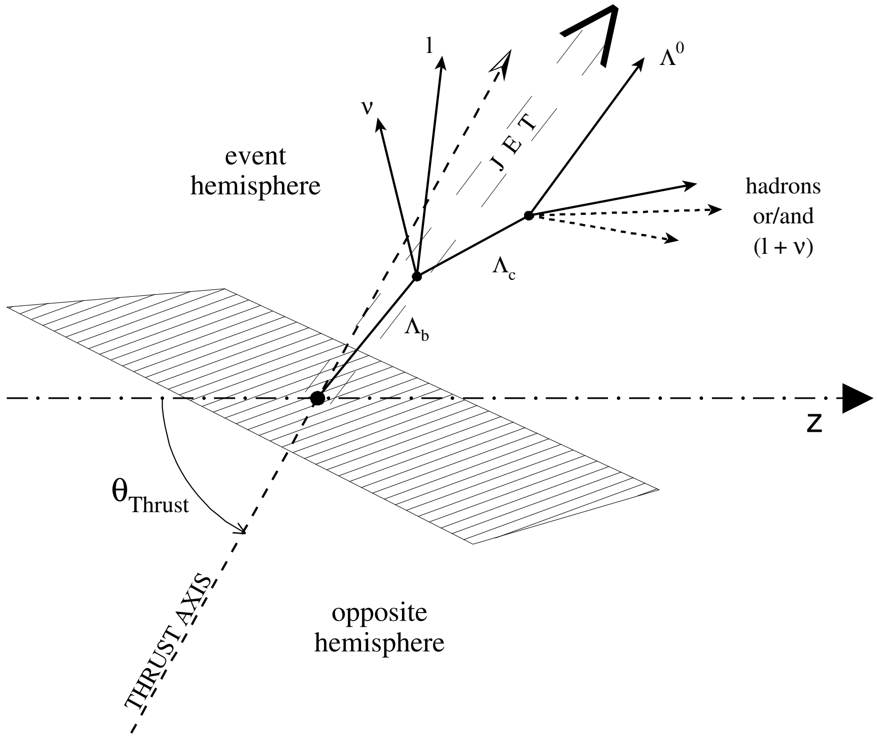

Figure 12: Topology of a typical event where Λ_b decays semileptonically and produces Λ^0 at the end of its decay chain. The event is subdivided into two hemispheres by the plane orthogonal to the thrust axis. The one containing the Λ_b decay products will be named the "event hemisphere" while the other one is referred to as the "opposite hemisphere". The neutral Λ^0 particle is reconstructed in its decay $\Lambda^0 \to p\pi^-$ via a pair of oppositely charged tracks pointing to a common vertex.

excluding the lepton candidate. The LUCLUS jet finding algorithm [79] has been used.

In addition electron candidates are rejected in cases where they match the photon conversion hypothesis tagged by a successful vertex fit with an oppositely charged electron candidate giving an invariant mass below 20 MeV/c^2. The compatibility of reconstructed lepton spectra in data and in Monte Carlo is discussed in section 5.5. The agreement is satisfactory.

Λ^0 reconstruction

Λ^0 candidates are reconstructed in the channel $\Lambda^0 \to p\pi^-$. This decay mode has a high branching fraction of $(63.9 \pm 0.5)\%$ [19]. The standard DELPHI reconstruction

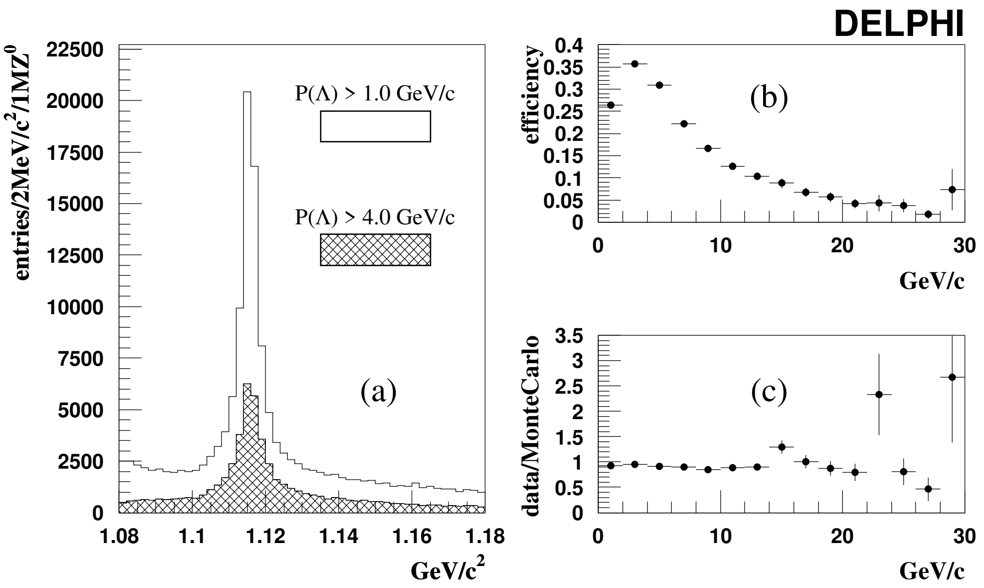

Figure 13: Λ^0 reconstruction in DELPHI; a) the $(p\pi)$ invariant mass distribution for the Λ^0 candidates reconstructed in DELPHI. The number of entries is normalized to 1 million hadronic Z^0 events. The hatched histogram gives the contribution from Λ^0 candidates with momenta above 4.0 GeV/c; b) the reconstruction efficiency as a function of Λ^0 momentum; c) the efficiency ratio ($\frac{data}{MonteCarlo}$) as a function of Λ^0 momentum; The evaluation is done for all Λ^0's where θ of the flight direction lies between 30° and 150°. The efficiency includes the loss coming from ≈35% of Λ^0's decaying into $n\pi^0$.

algorithm [54] considers all reconstructed distinct vertices of two oppositely charged tracks. The vertex defined by each pair is determined by minimizing the χ^2 obtained from the distances (and their errors) from the vertex to the extrapolated tracks. The Λ^0 candidates have to satisfy the following requirements:

- $\Delta\phi < (0.01 + 0.02/p_t)$rad, where $\Delta\phi$ is the angle in the xy plane between the Λ^0 momentum and the line joining the primary Z^0 decay vertex and the Λ^0 decay vertex, p_t is the transverse momentum of the Λ^0 candidate relative to the beam axis, in GeV/c,
- $R > 4\sigma$, where R and σ are respectively the reconstructed distance and its error between the primary and Λ^0 vertices in the xy plane,
- the χ^2 probability of the Λ^0 vertex fit is larger than 0.01,
- the transverse momentum of each particle of the Λ^0 with respect to the line of flight is greater than 0.02 GeV/c,

- when the reconstructed Λ^0 vertex is beyond the Vertex Detector radius, there must not be any VD signal associated to either of the Λ^0 tracks,

- probability to observe the Λ^0 decay within the fitted distance should be between 0.02 and 0.95,

- $m_{p\pi} < 1.3$ GeV/c^2, where the invariant mass is calculated attributing the proton mass to the higher momentum particle.

The background coming from the real K^0's is suppressed by requiring that an absolute value of the mass pull[1] for the K^0 hypothesis is either greater than three or is at least greater than the corresponding absolute mass pull for the Λ^0 hypothesis. The background from converted photons is reduced by requiring that the mass for the e^+e^- hypothesis is larger than 0.16 GeV/c^2.

In the analysis presented here only Λ^0 candidates with $p_\Lambda > 4$ GeV/c are selected. This requirement suppresses numerous low energy Λ^0's from fragmentation.

To extract the final signal of the Λ_b baryons Λ^0 candidates with an invariant mass of the pπ^- system in the range (1.108;1.128) GeV/c^2 have been used. It corresponds to a window of ± 8 MeV/c^2 around the nominal Λ^0 mass extended by 4 MeV/c^2 from the higher mass side. This extension is to account for the mass tail coming from the imperfection of the high momentum Λ^0 reconstruction.

Figure 13a shows the (pπ) system mass spectrum for the reconstructed Λ^0 candidates with momenta above 1.0 GeV together with the contribution from the energetic Λ^0's. As shown in Fig. 13b the reconstruction efficiency strongly depends on the Λ^0 momentum. It reaches its maximum ($\approx$35%) around 3.5 GeV/c and then drops systematically with increasing Λ^0 momentum. The mean efficiency for Λ^0's with momentum above 4.0 GeV has been found to be 20% . The limited efficiency to reconstruct energetic Λ^0's in the DELPHI experiment is mostly related to the small dimensions of the TPC detector (outer radius = 111 cm) as compared to the long Λ^0 lifetime ($c\tau = 7.89$ cm [19]). Moreover, the Λ^0 decay opening angle is fairly small due to the little energy available ($m_\Lambda - m_{\mathrm{p}} - m_\pi = 38$ MeV/c^2), making it again more difficult to separate proton and pion tracks from a prompt Λ^0 if only a small part of these tracks are measured.

The comparison between data and Monte Carlo (Fig. 13c) shows no significant discrepancy in the momentum dependence of the Λ^0 reconstruction efficiency.

---

[1] Pull is defined as the shift of a measured quantity from its nominal value divided by the error of the measurement.

b tagging

The algorithm to tag the reaction $e^+e^- \rightarrow Z^0 \rightarrow b\bar{b}$, described in [80], is based on a distinct long b hadron lifetime identified using the large track impact parameters of the decay products. The method profits from the good performance of the DELPHI silicon Vertex Detector (VD) described in 2.1.

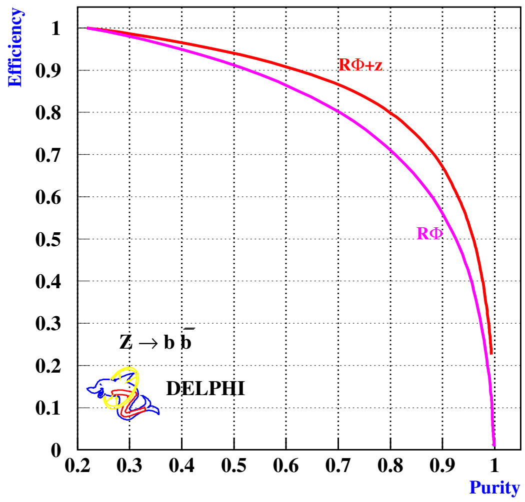

Figure 14: The efficiency and purity of the tagged b sample for different values of the cut on $\mathrm{P}_{b-\mathrm{TAG}}$ as obtained in DELPHI [81]. The lower curve shows the tagging performance when only an $R\phi$ measurement is available.

Hadrons containing b quarks have a long lifetime whose average value, according to the latest measurements, is around 1.6 ps (see Introduction for the exact numbers). Moreover, they are massive which causes their decay products to have large impact parameters relative to the e^+e^- interaction point (primary vertex). It should be noted here, that experimental measurements of the b-baryon lifetime show a significantly shorter lifetime of around 1.2 ps, which still remains an unsolved theoretical puzzle. Nevertheless, both b-mesons and b-baryons live long enough to produce secondary particles with impact parameters significantly large compared to the detector resolution. On this basis events in which b quarks are produced can be distinguished from the other hadronic events.

The procedure to tag b events uses all charged particles satisfying certain requirements for their reconstruction quality and consists of three main steps:

1. First the position in space of the primary Z^0 decay is determined using all charged particles being consistent with a common vertex and with the e^+e^- interaction point constrained with the beam position.

2. Next each charged particle is assigned an impact parameter with respect to the reconstructed primary vertex. It is defined as a distance of the closest approach of the track to the primary vertex. The sign of the impact parameter is positive if the vector joining the primary vertex to the point of closest approach of the track makes an angle of less than 90° with the direction of the jet to which the track belongs. Otherwise the sign is negative. The impact parameters in the $R\phi$ and Rz planes are evaluated separately but are given a common sign for a given track. With such a definition it follows that some particles from the decays of b-hadrons should have significant positive impact parameters, whereas all other charged particles should contribute to impact parameter distribution symmetrically around zero. On top of that, for each track a significance S is defined as a ratio of the impact parameter to its error.

3. Finally the b tagging algorithm itself can be applied. It uses a predefined probability function $P(S)$, which is the probability for a charged particle from the primary interaction to have a significance with absolute value S or greater. The N-track probability is defined as:

$$P_N = \Pi \cdot \sum_{j=0}^{N-1} (-\ln \Pi)^j / j!, \qquad \text{where} \qquad \Pi \equiv \prod_{i=1}^{N} P(S_i) \tag{0.31}$$

   This variable gives the probability for a group of N tracks all to come from the primary vertex. By construction, distribution of P_N is flat for groups of tracks from the primary vertex, while for b-hadron decay products has a sharp peak at zero.

The N-track probability determined for all tracks with positive significance is the variable used for tagging b events. It will be hereafter called a b-tag probability ($\mathrm{P}_{b-\mathrm{TAG}}$). The cut on $\mathrm{P}_{b-\mathrm{TAG}}$ determines the b efficiency and purity of the selected event sample. Figure 14 shows the efficiency and purity of the tagged sample depending on the value of the cut obtained in DELPHI for the years '94 and '95. Since in 1993 the VD was still single-sided (only $R\phi$ readout available) the lower curve in Fig. 14 should be considered as a good approximation of the b tagging performance in that year.

$\Lambda^0 l$ correlations

The signal of the Λ_b semileptonic decay is extracted using correlations between reconstructed Λ^0 candidates and identified charged leptons found in the same hemisphere. As already explained in section 4.1 Λ_b decays contribute uniquely to the *right-sign* $\Lambda^0 l$ combinations. Moreover, since the vast majority of background has no preferred charge

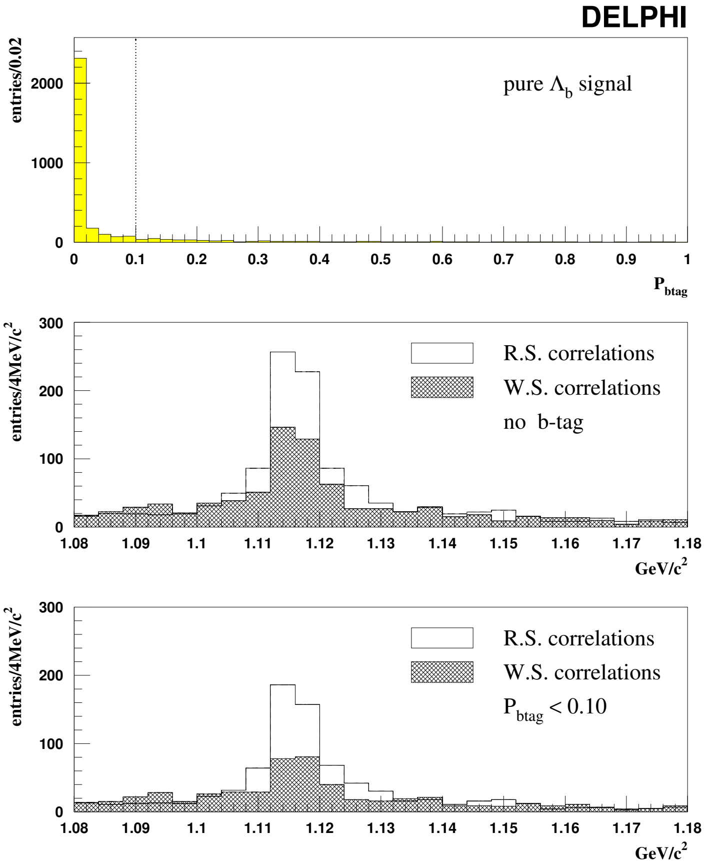

Figure 15: The upper plot gives the probability distribution of the b-tagging algorithm corresponding to a pure sample of Λ_b simulated events. The dotted line indicates the value of the cut used in the analysis. The two lower plots show the pπ mass distribution for Λ^0 candidates correlated to a charged lepton before and after the cut on the b-tagging probability.

correlation, the excess of *right-sign* events over the *wrong-sign* ones can be directly related the Λ_b signal.

The initial sample of $\Lambda^0 l$ pairs still contains a large fraction of background events mainly due to Λ^0 baryons from fragmentation and from non-b events. To reduce this background the following kinematical cuts have been applied:

- $m(\Lambda^0 l) \in (2.0; 4.5)$ GeV$/c^2$,
- $p(\Lambda^0 l) > 9.0$ GeV$/c$,
- $\measuredangle(\vec{\mathbf{p}}_l, \vec{\mathbf{p}}_\Lambda) < 90°$,

- $\sphericalangle(\vec{\mathbf{p}}_{\Lambda+l}$,thrust direction) $< 45°$.

The first two cuts select massive $\Lambda^0 l$ systems originating from a common prompt source which most probably is a b baryon. The next two cuts are fairly loose and mainly guard against accidental combinations where either the lepton or the Λ^0 belongs to a distinct hard gluon jet.

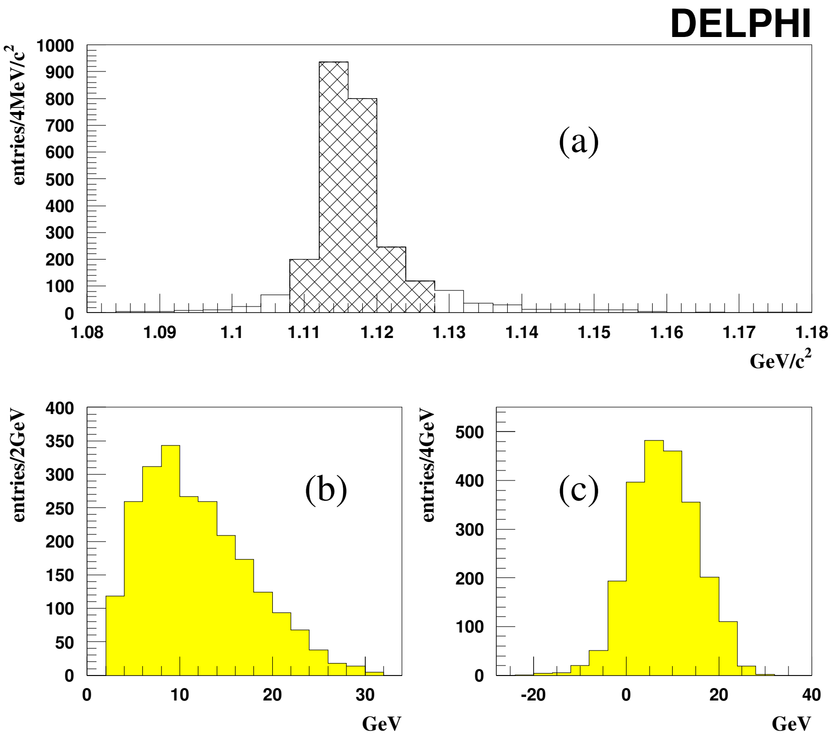

Figure 16: Signal from the genuine Λ_b semileptonic cascade decay $\Lambda_b^0 \to l^-\bar{\nu}_l\Lambda^0 X$; (a) the (p$\pi$) system invariant mass distribution for the reconstructed Λ^0's, hatched region shows the mass range from which we accept Λ^0 candidates; (b) energy spectrum of reconstructed charged leptons; (c) energy spectrum of reconstructed neutrinos.

On top of the above kinematical cuts a b tagging algorithm (see section 5.2) with the probability cut $P_{b-TAG} < 0.1$ was applied to the selected event sample. The Monte Carlo distribution of the P_{b-TAG} for genuine Λ_b events and the impact of the b-tag cut on the Λ_b signal in the data are shown in Fig. 15. This cut suppresses $\approx$40% of the background at the price of about 15% signal attenuation which corresponds to a drop of the background fraction from 58% to 48% .

Figure 16a shows the (pπ) system invariant mass distribution for the genuine signal of the cascade decay $\Lambda_b^0 \to l^-\bar{\nu}_l\Lambda^0 X$ reconstructed in the simulation. The correspond-

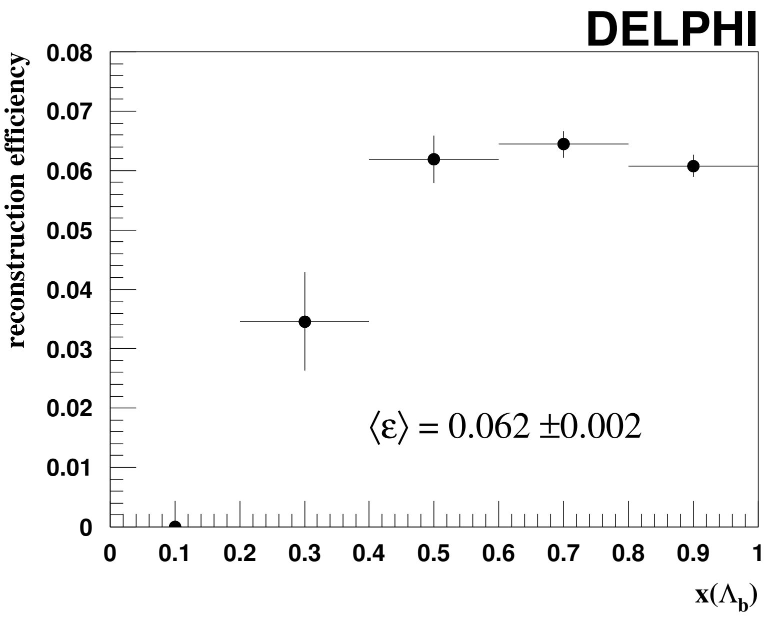

Figure 17: Efficiency of the $\Lambda_b^0 \to l\nu\Lambda^0 + X$ event reconstruction after the complete analysis. $x(\Lambda_b) = E_{\Lambda_b}/E_{\text{beam}}$.

ing reconstructed charged lepton and neutrino spectra are given in figures b and c. The measured energy distribution is a convolution of the original spectrum and the reconstruction resolution. Momenta of charged particles are measured directly through the track curvature as was described in section 2.1. What follows, in case of charged leptons the finite resolution of the energy reconstruction is negligibly small compared to the statistical fluctuation of the genuine spectrum. In contrast, the neutrino energy is not directly accessible experimentally. It has to be estimated on the basis of the missing energy in the event hemisphere as will be presented in detail in section 5.5. The algorithm leads, however, to a large error on the reconstructed neutrino energy. This limited resolution gives a significant contribution to the statistical error of the polarization measurement.

The estimated reconstruction efficiency as a function of the fraction of the beam energy carried by the Λ_b is shown in Fig. 17. The estimation is performed for events satisfying general selection criteria (described in section 5.1) with Λ_b decays where p(l)>3.0 GeV/c and p(Λ^0)>4.0 GeV/c. The corresponding mean reconstruction efficiency is found to be 0.062 ±0.002.

The reconstructed Λ^0 mass distributions for *right-sign* and *wrong-sign* $\Lambda^0 l$ charge correlations observed in the data are shown in Fig. 18. The excess of *right-sign* correla-

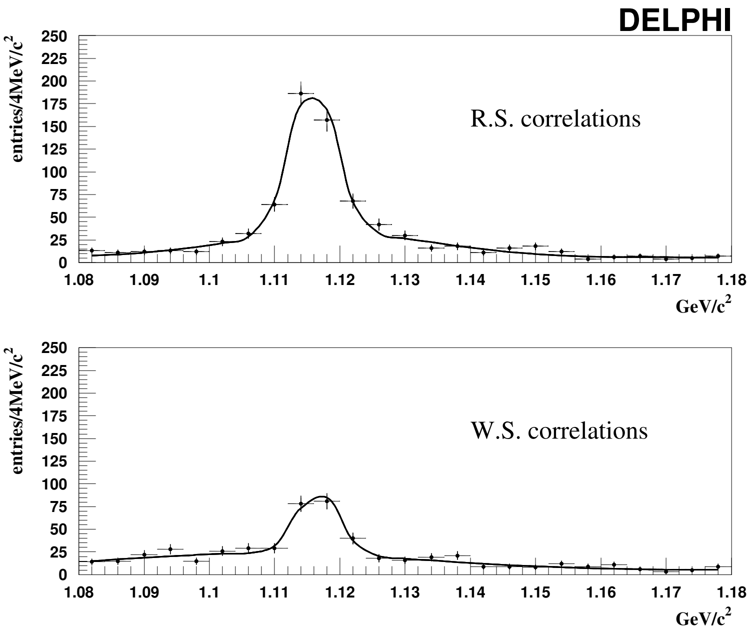

Figure 18: (pπ) mass distributions for Λ^0 candidates correlated with an identified high p$_T$ lepton in 1993–1995 data. The excess of *right-sign* over *wrong-sign* events is attributed to the b baryon signal. The curves are the result of the double-Gaussian fits.

tions over the *wrong-sign* ones in the Λ^0 mass peak amounts to 271 $\pm$22 Λ_b candidates. The corresponding Λ^0 mass distributions for *right-sign* and *wrong-sign* correlations obtained from over 4×10^6 $q\bar{q}$ Monte Carlo events are shown in Fig. 19. They reproduce well the signal observed in the data.

5.3 Background estimation and subtraction

To extract the average charged lepton and neutrino energies for the Λ_b signal, both the background fraction and the corresponding background average energies in the *right-sign* sample have to be known. As will be shown in this section, these characteristics can be extracted directly from the *wrong-sign* sample.

Background composition

In the following we will show that the background contained in the *right-sign* sample is to a good approximation mimicked by the *wrong-sign* sample.

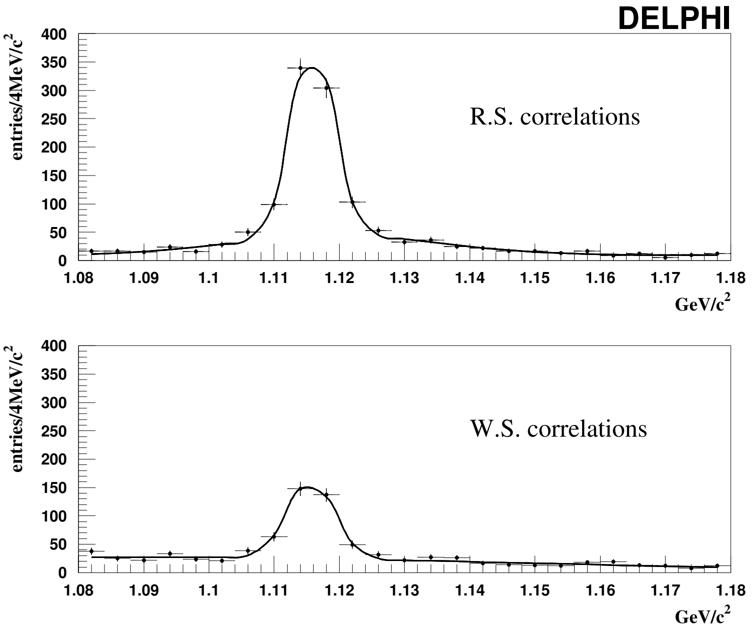

Figure 19: (pπ) mass for the Λ^0 candidates correlated with an identified high p_T lepton obtained from the simulation. The curves are the result of the double-Gaussian fits.

Except for a small fraction of particular physics processes the background consists to a large extent of accidental combinations between leptons (mainly from b) and Λ^0s from fragmentation or fake ones (background to the Λ^0 signal). The *right-sign* and *wrong-sign* Monte Carlo sample composition is shown in Fig. 20 and summarized in Table 3.

As has already been mentioned, the genuine decay $\Lambda_b \to l\nu\Lambda^0 X$ contributes only to the *right-sign* correlations. However, b-baryons can be the source of a background as well. In Table 3 there are the following three categories of the baryonic background:

1. $X_b \to l\nu X$ — where a true lepton from the baryon decay has been reconstructed but the Λ^0 is either fake or does not come from the b-baryon cascade. This category is almost equally distributed among the two sign correlations. A priori there should be a small enhancement in the *wrong-sign* due to fragmentation $\bar{\Lambda}^0$'s co-produced with the b baryon. However, this source is highly suppressed in the selection and has been found to be negligible.

2. $X_b \to \Lambda^0 X$ — where a true Λ^0 from the baryon cascade has been reconstructed but the lepton is either misidentified or does not come from the b semileptonic de-

event category	Right-Sign	Wrong-Sign
$\Lambda_b \to l\nu\Lambda^0 X$	437±21	—
b–baryons $X_b \to l\nu X$	52±8	56±7
b–baryons $X_b \to \Lambda^0 X$	18±4	28±5
b–baryons $X_b \to X$	9±3	3±2
B mesons	303±17	257±16
c–jets	39±6	48±7
u, d, s or g	37±6	40±6
total background	461±21	429±21

Table 3: Monte Carlo composition of the *right-sign* and *wrong-sign* event samples after applying all selection criteria.

cay. Here there might be two physical sources of definite sign combinations. The first one, b-baryon $\to$ c-baryon $\to$ $l^+\nu_l\Lambda^0 X$ where the lepton from the semileptonic c decay has been selected, is a source of *wrong-sign* combinations. It is highly suppressed by the requirements of a high lepton p_T and a mass for the $\Lambda^0 l$ system to exceed 2 GeV$/c^2$. Therefore, its contribution to the total background does not exceed 2% . The second one, b-baryon $\to \tau\bar{\nu_\tau}\Lambda^0 X$ where $\tau \to \nu_\tau l \bar{\nu_l}$, is in turn a source of *right-sign* combinations. The BR($b \to \tau^- \to l^-$) has been experimentally estimated to be (0.7 ± 0.2)% [16] and is not negligible. A certain attenuation of this signal is obtained by a requirement of the high momentum of the lepton since the lepton from the τ cascade is less energetic. From the Monte Carlo estimation τ background gives a small contribution (below 2%), but since it is characterized by exceptionally high missing energy (low y values) it can lead to a perceptible systematic shift. The exceptionally high missing energy comes from the fact that in the process there are three escaping neutrinos: a $\bar{\nu_\tau}$ from the semileptonic b decay to a τ and a $\nu_\tau + \bar{\nu_l}$ from the τ decay.

3. $X_b \to X$ — where neither the lepton from the b decay nor the Λ^0 from its cascade have been found. This category is very poorly populated and besides should not contain any bias towards either sign combination.

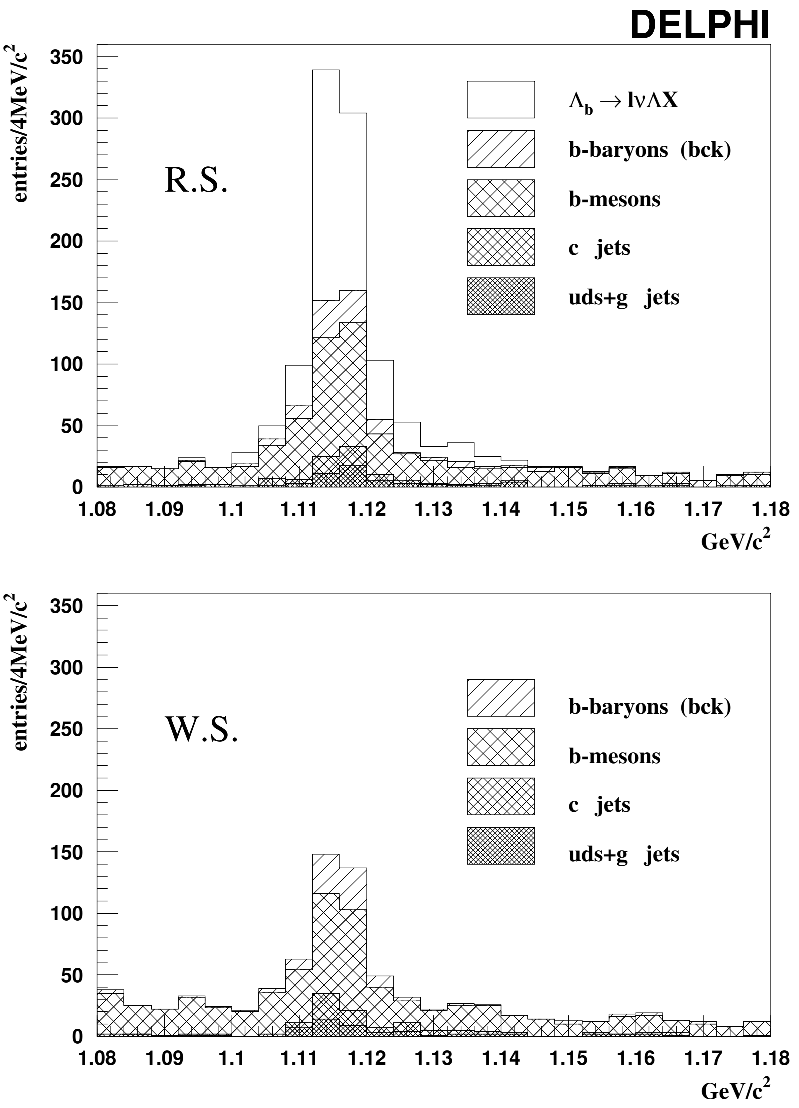

Figure 20: Monte Carlo composition of the *right-sign* and the *wrong-sign* event samples after applying all selection criteria. The signal is expressed in terms of $(p\pi)$ mass distributions for Λ^0 candidates correlated with an identified high p_T lepton.

As it is shown in Table 3 majority of the background comes from B mesons. Most of it are accidental combinations which are not biased towards either of two sign combinations. However, in the meson sample we also find sources of possible biases between *right-sign* and *wrong-sign* samples. As seen in the table they amount to some 10% of the total background. The excess in the *right-sign* sample originates from true leptons

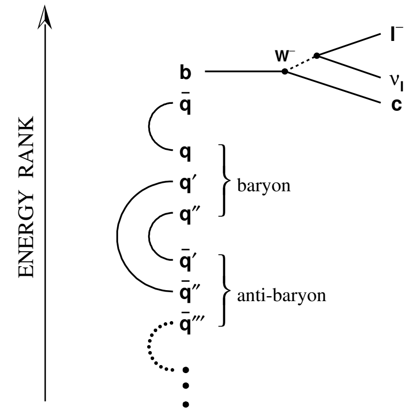

Figure 21: A simplified picture of the hadronization leading to the strong energy ranking of the fragmentation products.

from semileptonic B decays paired with prompt Λ^0's from fragmentation. In the fragmentation baryons are always produced in baryon anti-baryon pairs completely symmetrically. However, the strong energy ranking built-in to the Monte Carlo model has the effect that an energetic baryon from fragmentation most probably contains the anti-partner of the light quark building the B meson [82]. A simplified picture showing this mechanism is given in Fig. 21. Therefore, by asking for Λ^0's momentum>4.0 GeV/c we favour pairs of the type: $(\bar{B} = b\bar{q}) + (qq'q'' = \text{baryon})$ which contribute to the *right-sign* sample. In this picture the anti-baryon from fragmentation has to be lower in the energy rank and hence has smaller probability to pass the selections. Obviously we cannot directly assume that the same mechanism exists in reality[1]. Therefore, this phenomenon can be only treated as a source of systematic uncertainty and as such will be included in the final error. Semileptonic B decays, such as $B \to \Lambda_c \bar{N} l \nu X$ (where $\bar{N}$ is an antibaryon) could also give rise to an excess of the *right-sign* combinations. The actual branching fraction for such processes is yet not measured but from the available limits the contribution of this background has been estimated to be negligible [45]. In fact, in the Monte Carlo we do not observe any events of this type.

The third class of the background is the one originating from a c quark. Apart from accidental combinations it contains $\Lambda^0 l$ pairs from the process c-baryon $\to \Lambda^0 X$ which contribute to the *wrong-sign* sample. Their contribution is highly suppressed by the cut on the lepton p_T and by the b-tagging and should stay at the 2% level.

[1] One could think of measuring it in the data using e.g. sign correlation between reconstructed D^*'s and Λ^0's or protons as a function of the energy of the latter. This, however, deserves a separate analysis and has not been done up to now.

MC background	Right-Sign (GeV)	Wrong-Sign (GeV)
average E_l	9.70±0.26	9.24±0.26
average E_ν	6.05±0.35	5.88±0.35
y	1.60±0.10	1.57±0.10

Table 4: Average reconstructed charged lepton and neutrino energies and their ratio y in *right-sign* and *wrong-sign* Monte Carlo background.

Finally, the last class contains $\Lambda^0 l$ pairs reconstructed in the u, d, s or gluon jets. These combinations are purely accidental and hence are equally distributed among *right-sign* and *wrong-sign* samples.

Concluding, apart from the limited physics bias the total *right-sign* and *wrong-sign* background samples show an agreement. Similarly, the corresponding lepton energy distributions should be compatible in the two cases. Average energies of the charged lepton and the neutrino in the two background samples for the MC events are given in Table 4. In particular the resulting y values stay in a good agreement.

Possible deviations to the polarization measurement arising from the particular physics processes discussed above will be summarized in section 6.3 and will contribute to the systematic error.

Background subtraction

Having verified the assumption that the *right-sign* background is well reproduced by the *wrong-sign* sample it is possible to evaluate the properties of the genuine Λ_b component. In particular the average charged lepton energy and the average neutrino energy originating from the Λ_b semileptonic decay can be obtained using the following background subtraction:

$$\langle E_{l,\nu} \rangle = \frac{1}{1 - f_{bck}} (\langle E_{l,\nu}^{R.S.} \rangle - f_{bck} \langle E_{l,\nu}^{W.S.} \rangle) \tag{0.32}$$

where $\langle E_{l,\nu}^{R.S.} \rangle$ and $\langle E_{l,\nu}^{W.S.} \rangle$ are the average charged lepton or neutrino energies measured in the *right-sign* and in the *wrong-sign* samples respectively. f_{bck} is the background fraction defined as:

$$f_{bck} = \frac{\mathrm{N}^{W.S.}}{\mathrm{N}^{R.S.}} \tag{0.33}$$

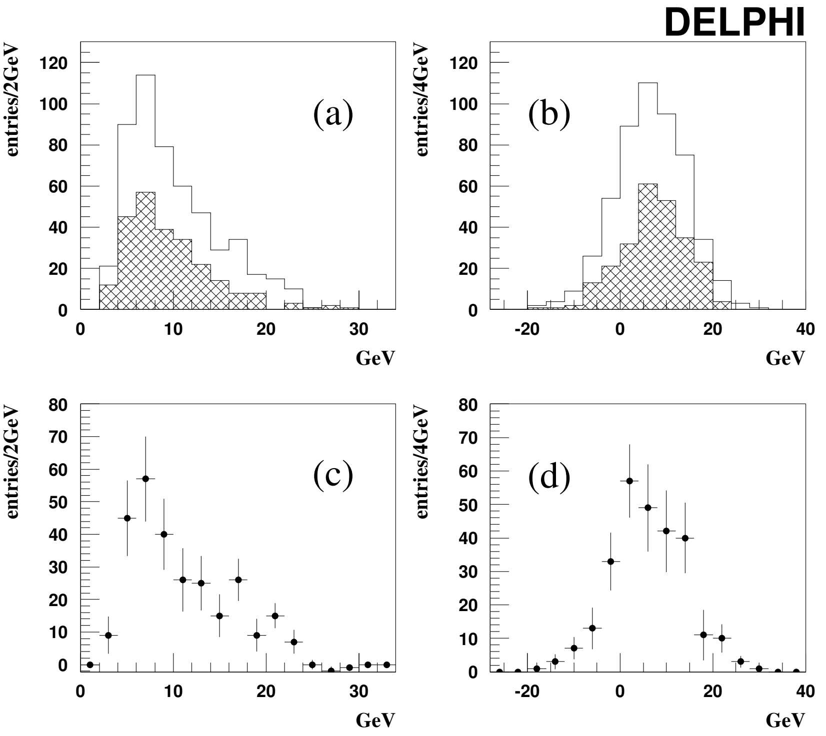

Figure 22: Lepton energy spectra for the final $\Lambda^0 l$ sample found in data. Plots (a) and (c) show the charged lepton energy while plots (b) and (d) give corresponding distributions for the neutrino. The upper plots show distributions for *right-sign* (blank histogram) and *wrong-sign* (hatched histogram) $\Lambda^0 l$ pairs. The lower plots show the corresponding background subtracted spectra for the Λ_b signal (*right-sign* $-$ *wrong-sign*).

where $N^{R.S.}$ and $N^{W.S.}$ are the number of selected events found in the *right-sign* and *wrong-sign* samples respectively.

Fig. 22 shows the charged lepton and neutrino energy spectra for both *right-sign* and *wrong-sign* samples and for the Λ_b signal obtained after the background subtraction. Figure 23 shows the same distributions obtained from the Monte Carlo. The spectra especially in the *wrong-sign* look similar. However, in Monte Carlo there seems to be a harder fragmentation function to Λ_b baryon than observed in the data. It is manifested in the harder charged lepton spectrum. The possible impact of the fragmentation function on the polarization measurement will be covered in section 6.3 where the systematic error is estimated.

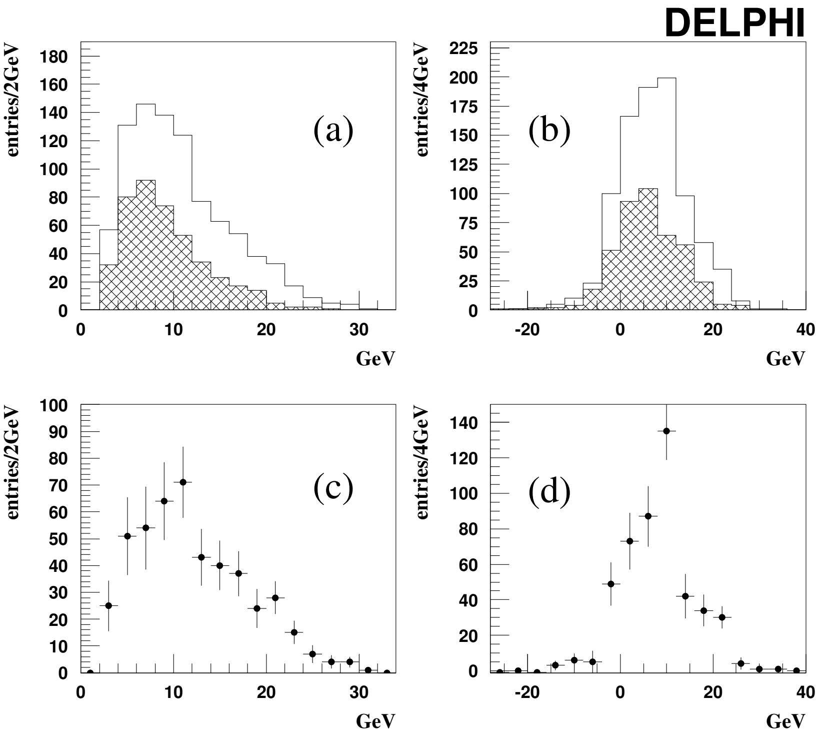

Figure 23: Lepton energy spectra for the final $\Lambda^0 l$ sample found in the Monte Carlo. Plots (a) and (c) show the charged lepton energy while plots (b) and (d) give corresponding distributions for the neutrino. The upper plots show distributions for *right-sign* (blank histogram) and *wrong-sign* (hatched histogram) $\Lambda^0 l$ pairs. The lower plots show the corresponding background subtracted spectra for the Λ_b signal (*right-sign* – *wrong-sign*).

5.4 B^0 signal selection

Here we will briefly describe the selection of the B^0 meson semileptonic decays via the process $B^0 \longrightarrow D^* l^+ \nu_l$. As already argued in section 3.2 mesons should not retain any polarization of the primary b quark. Therefore, the meson decays can serve as an independent test of the analysis procedure. In other words the polarization measured on the B^0 sample should be consistent with zero.

The D^* mesons are reconstructed in the channel $D^* \to D^0 \pi^+_{\mathrm{soft}}$ where $D^0 \to K^- \pi^+$. The first decay has a high branching fraction of $\cong$68% and the second one accounts for $\cong$4% of D^0 decays [19].

The B^0 selection was performed on events satisfying the general requirements described in section 5.1. D^0s are reconstructed using all pairs of oppositely charged tracks having at least two VD hits each. On such pairs the following kinematical cuts were applied:

- $P_K > 1.0$ GeV
- $P_\pi > 1.0$ GeV
- successful $K\pi$ vertex fit with probability > 0.001
- $P_{D^0} > 5.0$ GeV
- $> 2\sigma$ incompatibility with the primary vertex
- flight distance < 3.0 cm
- $\sphericalangle(\vec{\mathbf{p}}_{D^0}$,line of flight$) < 10°$
- $m(D^0) \in (1.80; 1.92)$ GeV$/c^2$

Next, the D^0 candidates were combined with a pion candidate (a charged track) having momentum between 0.35 and 3.5 GeV$/c$. The D^* signal is observed as a peak in the $\Delta m = m(D^0\pi) - m(D^0)$ distribution for the π candidates with a charge opposite to the charge attributed to K from the D^0. The D^* signal peak is defined for $\Delta m \in (1.815;1.915)$ GeV$/c^2$.

Next, the D^* candidates were correlated with high p_T leptons found in the same hemisphere. Lepton selection was the same as that described in 5.2. The kinematical cuts on the D^*l pairs were the following:

- $m(D^0 l) \in (2.0; 5.2)$ GeV$/c^2$
- $\sphericalangle(\vec{\mathbf{p}}_l, \vec{\mathbf{p}}_{D^0}) < 90°$
- $P_{b-TAG} < 0.10$

The D^*l^+ and $\bar{D}^*l^-$ pairs originate mainly from genuine B^0 meson semileptonic decays (BR($B^0 \longrightarrow D^*l^+\nu_l) = (4.4 \pm 0.4)\%$ [19]). These combinations will be called *right-sign*. Opposite sign combinations (*wrong-sign*) have a purely background origin. The Δm distributions for the *right-sign* and *wrong-sign* samples are shown in Fig. 24. In the Δm peak the excess in the *right-sign* sample amounts to 281 ± 7 B^0 candidates. Analogous plots obtained from the simulation of $b\bar{b}$ events are given in Fig. 25. The number of Monte Carlo $b\bar{b}$ events corresponds to twice the statistics of the real data. The observed signal scales well between data and Monte Carlo. However, the width of the Δm peak in the data is slightly bigger than in the Monte Carlo.

The $B^0 \longrightarrow D^*l^+\nu_l$ signal is very pure. This comes from the fact that there is no source of accidental D^*l combinations. D^*s are not copiously produced in the fragmentation as in the case of Λ^0 baryons. There is also no other competing process that could lead to D^*l pairs. The existing small background comes either from misidentified leptons or the combinatorial background to the D^* signal.

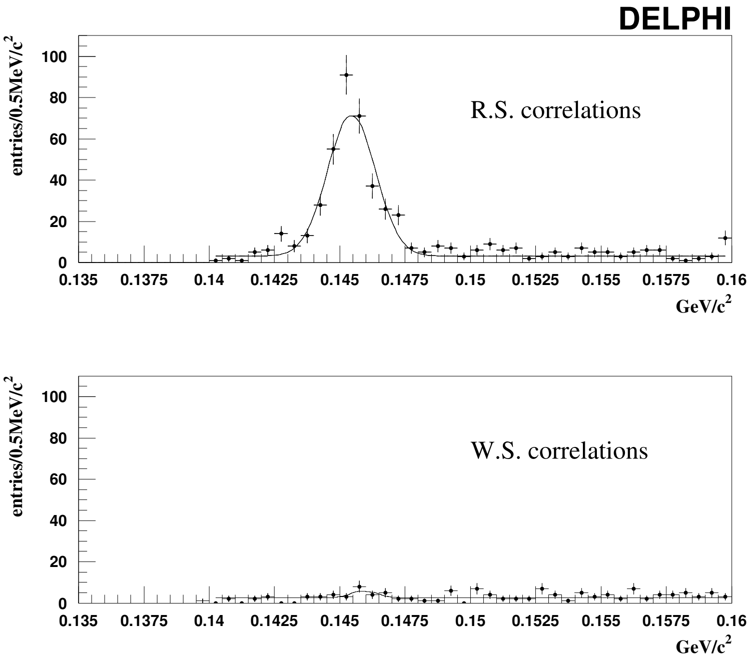

Figure 24: $\Delta m = m(D^0\pi) - m(D^0)$ distributions for the D^* candidates correlated with an identified high p_T lepton obtained in the 1993–1995 data. The curves are the result of Gaussian fits.

5.5 Neutrino energy reconstruction

The neutrino energy is measured as a missing energy ($E_{\rm miss}$) in the hemisphere containing the $\Lambda^0 l$ system (event hemisphere). To evaluate the hemisphere total visible energy the sum of all charged track energies and neutral energy deposits reconstructed in the DELPHI apparatus have been used. The neutrino energy is obtained from:

$$\begin{aligned} E_\nu &\approx E_{\rm miss} = E_{\rm TOT} - E_{\rm vis}^{\rm corr} \\ E_{\rm TOT} &= \frac{\sqrt{s}}{2} + \frac{(M^{\rm event})^2 - (M^{\rm oppo})^2}{2\sqrt{s}} \end{aligned} \tag{0.34}$$

where $E_{\rm vis}^{\rm corr}$ is the sum of all charged track energies and neutral calorimeter energy deposits in the event hemisphere ($E_{\rm vis}$) corrected for the detector inefficiencies. $E_{\rm TOT}$ is the total energy available in the event hemisphere. The lower equation results directly from the four-momentum conservation applied to the entire event. $M^{\rm event}$ and $M^{\rm oppo}$ are the event hemisphere invariant mass and the opposite hemisphere invariant mass respectively. $\sqrt{s}$ denotes the total energy in the center of mass of the colliding e^+e^- ($E_{\rm CM}$) and is equal to the Z^0 mass.

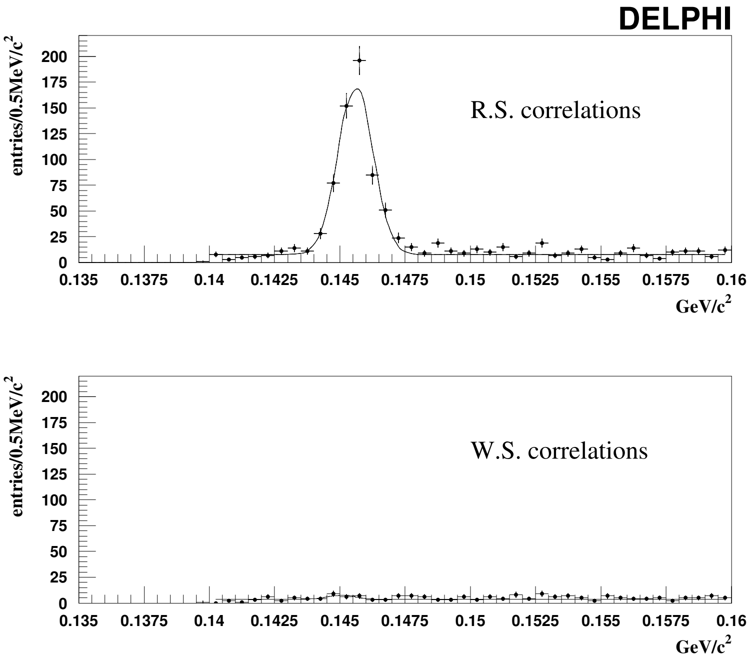

Figure 25: $\Delta m = m(D^0\pi) - m(D^0)$ distributions for the D^* candidates correlated with an identified high p_T lepton obtained from the simulation of $b\bar{b}$ events. The curves are the result of Gaussian fits.

Individual hits in multiple layers of both the electromagnetic calorimeters (HPC or FEMC) and hadronic calorimeters (HCAL) are clustered according to the spatial resolution of the given calorimeter to form bigger deposits which are likely to come from single particle showers. Then a matching between reconstructed charged tracks and the calorimeter showers is performed. The neutral deposits not associated to any charged track are assumed to originate from a neutral particle cascade. Together with all reconstructed charged tracks they contribute to the total visible energy $E_{\rm vis}$ and to the computation of the hemisphere masses $M^i_{\rm vis}$.

For the reconstruction of the hemisphere mass the following formula was found to be the best approximation;

$$M^i = M^i_{\rm vis} \frac{\sqrt{s}}{2E_{\rm vis}} \tag{0.35}$$

where $M^i_{\rm vis}$ is the hemisphere invariant mass calculated directly from the reconstructed charged and neutral particles as described above.

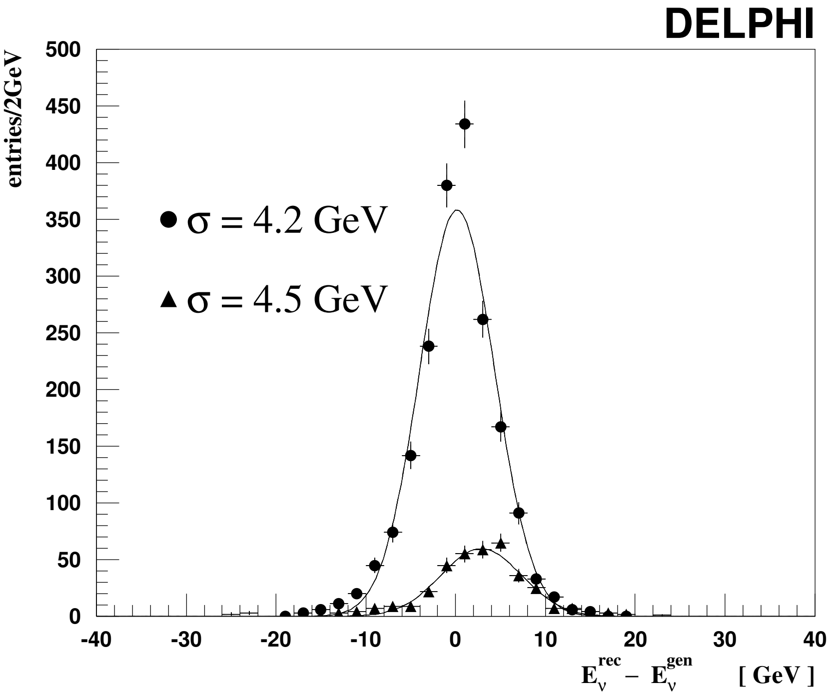

Figure 26: Final E_ν resolution obtained for Monte Carlo $\Lambda_b \to l\nu\Lambda^0 X$ events. Points show the contribution from hadronic Λ_c decays and triangles the contribution from semileptonic Λ_c decays.

In the ideal case E_{miss} should be equal to E_ν. In practice the energy resolution measured by a difference between the reconstructed and the generated neutrino energy $(E_\nu^{\text{rec}} - E_\nu^{\text{gen}})$ is distributed according to a wide Gaussian. The resolution of the neutrino energy reconstruction obtained in the Monte Carlo events with a Λ_b semileptonic decay is shown in Fig. 26. The two fits correspond to contributions from purely hadronic Λ_c decays and semileptonic Λ_c decays. Clearly, the two cases are considerably different since in the latter there is an additional neutrino from the Λ_c decay escaping from the apparatus. The fitted resolution amounts to 4.2 GeV and 4.5 GeV respectively. Moreover the E_ν residuals for hadronic Λ_c decays are nicely centered on zero while semileptonic Λ_c decay subsample shows a large offset of $\approx$2.8 GeV. The observed offset is equal to the average energy of the neutrino from the Λ_c decay. In the analysis presented here we have no handle to distinguish between hadronic and semileptonic Λ_c decays in the real data. Therefore the two contributions have been put together and certain assumptions are made about the fraction of Λ_c semileptonic decays with a Λ^0 produced in the final state. In the simulation after the whole signal selection we found (16$\pm$1)% of semileptonic Λ_c decays within inclusive $\Lambda_c \to \Lambda^0 + X$ decays. The

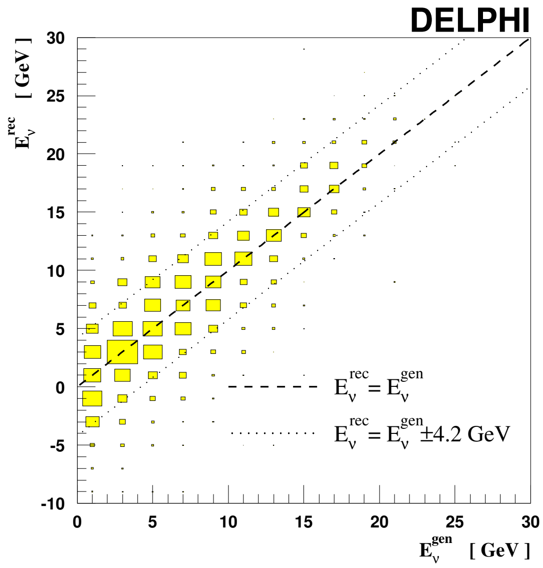

Figure 27: Scatter plot of the reconstructed E_ν versus the generated one in the simulated sample of Λ_b semileptonic decays. Semileptonic Λ_c decays are excluded. The dotted lines show the 1σ bound around the generated value.

$\langle \mathrm{E} \rangle$ (GeV)	data	Monte Carlo
$\mathrm{P}_{b-\mathrm{TAG}} < 0.01$	82.82±0.05	82.74±0.05
$\mathrm{P}_{b-\mathrm{TAG}} > 0.01$	83.12±0.03	83.20±0.03

Table 5: Comparison of the average total visible event energy reconstructed in the data and in the Monte Carlo. Events containing identified leptons with $p > 3.0$ GeV/c have been excluded.

uncertainty coming from the unknown fraction $\frac{BR(\Lambda_c \to l\nu\Lambda^0 X)}{BR(\Lambda_c \to \Lambda^0 X)}$ is taken into account in the systematic error. The neutrino energy estimation does not show any significant energy dependence. The scatter plot of the reconstructed energy versus the generated one is presented in Figure 27. The dotted lines indicate the assumed energy resolution fitted for the hadronic Λ_c decays as shown in Fig. 26.

As a next crucial step we have to make sure that there are no severe systematic differences in the missing energy evaluation between data and Monte Carlo. We do it using several samples. Here the global event selections described in section 5.1 are implied.

As a first approximation we compare total visible energies for events without any identified leptons with momentum above 3.0 GeV. The comparison is done on two different samples independent by their construction. In the first one a "tight" b-tagging (P_{b-TAG} <0.01) is required giving an over 85% pure b event sample. The second one is the complementary one consisting in 90% of non-b events (P_{b-TAG} >0.01). The example distribution for the b-tagged sample is shown in Fig. 28a. We observe a satisfactory agreement between data and Monte Carlo, the only difference being that the distributions in real data tend to be slightly wider. Hence for the neutrino energy reconstruction in data we increase the assumed resolution with respect to the one obtained from simulation. The 4.5 GeV will be taken. The results of the data/Monte Carlo comparison are summarized in Table 5. The observed discrepancies in the average energies stay at the 0.001 level and indicate a very good agreement between data and Monte Carlo. However, these numbers are obtained on highly inclusive samples and moreover do not contain possible distortions from the hemisphere separation. Thus they cannot be considered as an ultimate proof.

The next, more refined cross-check is done on the inclusive sample of b-hadron semileptonic decays. The sample is selected requiring an identified energetic lepton ($p > 3.0$ GeV/c) with a high p_T ($p_T > 1.0$ GeV) contained in a b-tagged event. The comparison is performed for two levels of tagging; ($P_{b-\mathrm{TAG}} < 0.01$) and ($P_{b-\mathrm{TAG}} < 0.10$) corresponding to b purities of ≈85% and ≈60% respectively. Since 90% of b's hadronize into mesons the inclusive sample should not retain any significant polarization as argued in 3.2. Therefore, the reconstructed lepton and neutrino energy spectra should be compatible in data and in Monte Carlo and in particular should result in the same y values. Plots 28b–e show the comparison of the charged lepton and of the hemisphere missing energy E_{miss} spectra reconstructed in data and in Monte Carlo in case of tight b-tagging ($P_{b-\mathrm{TAG}} < 0.01$). Plots in the left column correspond to the muon subsample while the ones in the right column correspond to the electron subsample. Both charged lepton spectra and E_{miss} spectra show a nice agreement between data and Monte Carlo. In addition, plots 28f and 28g give spectra of visible energy in the hemisphere opposite to the reconstructed lepton. In this hemisphere an additional requirement not to have any identified leptons with $p > 3.0$ GeV/c is applied. Here again data and Monte Carlo plots show almost perfect agreement. The detailed numerical results of the whole cross-check are summarized in Table 6. The table contains four quantities extracted for each sample:

1. average energy of the charged lepton (μ or e),
2. average missing energy in the lepton hemisphere obtained using the same algorithm as for the E_ν reconstruction,
3. ratio of the above two mean values which is the observable directly sensitive to polarization,

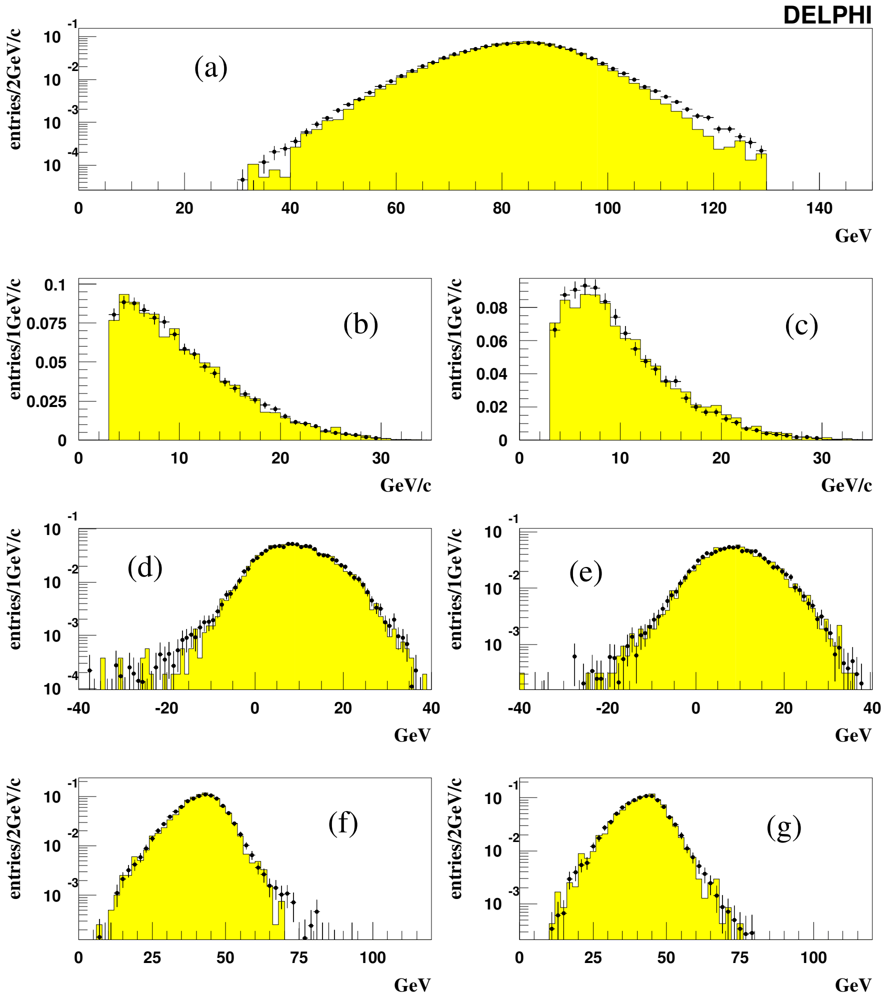

Figure 28: Comparison of different reconstructed energy spectra in the data and in the simulation. The Monte Carlo results are always presented as a shaded histogram and real data as points with error bars. The global event selections were applied (see section 5.1). (a) the total visible event energy in b-tagged events without identified leptons ($P_{btag} < 0.01$); (b) momentum spectrum of identified muons with $p > 3.0$ GeV/c and $p_T > 1.0$ GeV/c in b-tagged events; (c) momentum spectrum of identified electrons with $p > 3.0$ GeV/c and $p_T > 1.0$ GeV/c in b-tagged events; (d) missing energy in the muon hemisphere (sample like in b); (e) missing energy in the electron hemisphere (sample like in c); (f) visible energy in the hemisphere opposite to the muon (sample like in b) with the additional requirement of no identified leptons in this hemisphere; (g) visible energy in the hemisphere opposite to the electron (sample like in c) with the additional requirement of no identified leptons in this hemisphere.

$\langle E \rangle$ (GeV)	data	Monte Carlo
muons, $P_{b-\mathrm{TAG}} < 0.01$ $p > 3.0$ GeV/c, $p_T > 1.0$ GeV/c		
$\langle E \rangle_\mu$	10.38±0.07	10.41±0.07
$\langle E \rangle_{\mathrm{miss}}$	9.15±0.10	9.13±0.10
$y = \langle E \rangle_\mu / \langle E \rangle_{\mathrm{miss}}$	1.134±0.015	1.140±0.015
$\langle E \rangle^{\mathrm{oppo}}$	41.30±0.10	41.22±0.10
electrons, $P_{b-\mathrm{TAG}} < 0.01$ $p > 3.0$ GeV/c, $p_T > 1.0$ GeV/c		
$\langle E \rangle_e$	10.04±0.07	10.37±0.07
$\langle E \rangle_{\mathrm{miss}}$	8.88±0.10	9.06±0.10
$y = \langle E \rangle_e / \langle E \rangle_{\mathrm{miss}}$	1.131±0.015	1.145±0.015
$\langle E \rangle^{\mathrm{oppo}}$	41.67±0.10	41.69±0.10
muons, $P_{b-\mathrm{TAG}} < 0.10$ $p > 3.0$ GeV/c, $p_T > 1.0$ GeV/c		
$\langle E \rangle_\mu$	10.38±0.07	10.40±0.07
$\langle E \rangle_{\mathrm{miss}}$	9.12±0.10	9.22±0.10
$y = \langle E \rangle_\mu / \langle E \rangle_{\mathrm{miss}}$	1.138±0.015	1.128±0.015
$\langle E \rangle^{\mathrm{oppo}}$	40.92±0.10	41.06±0.10
electrons, $P_{b-\mathrm{TAG}} < 0.10$ $p > 3.0$ GeV/c, $p_T > 1.0$ GeV/c		
$\langle E \rangle_e$	10.08±0.07	10.34±0.07
$\langle E \rangle_{\mathrm{miss}}$	8.72±0.10	8.96±0.10
$y = \langle E \rangle_e / \langle E \rangle_{\mathrm{miss}}$	1.156±0.015	1.154±0.015
$\langle E \rangle^{\mathrm{oppo}}$	41.51±0.10	41.59±0.10

Table 6: Hemisphere energy reconstruction in the data and in the Monte Carlo. The opposite hemispheres ($\langle E \rangle^{\mathrm{oppo}}$) containing identified leptons with $p > 3.0$ GeV/c have been excluded.

4. average energy of the opposite hemisphere; events that have in the opposite hemisphere identified leptons with $p > 3.0$ GeV/c are excluded.

The two muon samples give almost perfect agreement in both lepton and neutrino spectra and finally in the extracted y value. The electron sample is a bit more difficult case as the electron identification is more complex, less efficient and finally more complicated to control. In the data the reconstructed electron spectrum is softer than in the simulation. It can be a result of either different background composition or an unequal efficiency function in data and Monte Carlo. The results rather indicate the latter scenario. The missing energy spectrum follows the discrepancy in the electron spectrum and together result in the y being compatible in data and MC within the statistical uncertainty. Anyhow, in the Λ_b signal all systematics coming from the different background compositions cancel out after the background subtraction described in 5.3. An additional data – Monte Carlo comparison of the energy estimation in the opposite hemisphere shows a nice agreement for all presented samples.

Considering muons as a more reliable probe we conclude that all data – Monte Carlo discrepancies stay within one standard deviation of the statistical uncertainty. Therefore, taking a conservative value of 1.5σ we can assume that our systematic error on E_ν should not exceed 200 MeV.

6 Polarization measurement results and error estimation

6.1 Measured value of the Λ_b polarization

The Λ_b polarization is determined from the value of the R_y observable which is the ratio of y values measured in data and in the reference simulation where the Λ_b decays are unpolarized. As was explained in section 4.2 y is the ratio of the average charged lepton energy $\langle E_l \rangle$ and the average neutrino energy $\langle E_\nu \rangle$ obtained after background subtraction. As an unpolarized reference the dedicated Λ_b enriched Monte Carlo has been used. As already mentioned in the beginning of chapter 5 it is highly populated and contains practically no background. Therefore, in this simulated sample the reference y^{MC} for the genuine Λ_b signal is determined with a high statistical sensitivity. The simulated unbiased $q\bar{q}$ events have been used only as an independent cross-check of the obtained results.

sample	Λ_b enriched MC	$q\bar{q}$ MC	1993–1995 data
# of Λ_b candidates	2259±13	469±29	271±22
f_{bck}	0.034±0.004	0.48±0.03	0.48±0.04
$\langle E_l \rangle$ (GeV)	11.91±0.13	12.18±0.39	10.52±0.52
$\langle E_\nu \rangle$ (GeV)	8.16±0.16	8.17±0.57	5.87±0.74
y	1.46±0.04	1.49±0.12	1.79±0.25
R_y	1.0	1.02±0.09	1.23±0.17
P	0.0	$-0.05^{+0.23}_{-0.20}$	$-0.48^{+0.35}_{-0.27}$

Table 7: Analysis results obtained for the reference Λ_b Monte Carlo, the simulated unbiased $q\bar{q}$ events and the data. The quoted errors are statistical only.

The results obtained for the reference Λ_b Monte Carlo, the simulated unbiased $q\bar{q}$ events and the data are summarized in Table 7. Due to high statistics and lack of background the MC reference (y^{MC}) has been evaluated with an almost negligible statistical error. The corresponding R_y and polarization P for the Λ_b enriched sample are by definition equal to one and zero respectively. The whole analysis applied to the simulation

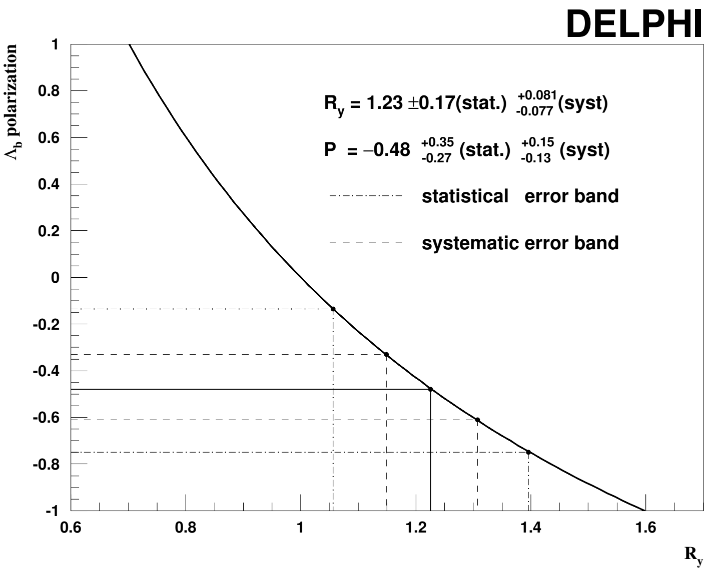

Figure 29: Result extraction from the calibration curve.

of the unbiased $q\bar{q}$ events gives a result which is quite compatible with zero. Moreover, all observables are within their errors in good agreement with the ones obtained from the background free reference MC. This result additionally confirms the validity of assumptions about the background behaviour and its subtraction done in section 5.3. However, the y extracted from the unbiased $q\bar{q}$ simulated events still carries with it a considerable statistical error and hence cannot be directly used as the unpolarized reference. The last column of Table 7 gives relevant results extracted from the data. The result reads:

$$R_y = \frac{y^{data}}{y^{MC}} = 1.23 \ \pm 0.17(\text{stat.}) \ \pm 0.08(\text{syst.}) \tag{0.36}$$

The polarization is extracted by comparing the obtained R_y value with the calibration curve as shown in Fig. 29. The calibration curve is exactly the one obtained as a result of a fit to simulated data points in Fig. 10 of chapter 4. The curve gives the correspondence between the reconstructed R_y and the Λ_b polarization as determined from the Monte Carlo. Here, the axes have been swapped for better visualization. Figure 29 shows in addition a propagation of the statistical and systematic errors from R_y to P_{Λ_b}. It explains why for the polarization they become asymmetric.

The Λ_b polarization is found to be:

$$P_{\Lambda_b} = -0.48 \,^{+0.35}_{-0.27}(\mathrm{stat.}) \,^{+0.15}_{-0.13}(\mathrm{syst.}) \tag{0.37}$$

The statistical and systematic errors have been derived as described in section 6.2 and section 6.3 respectively.

From the theoretical predictions presented in Fig. 10 we should expect a rise of the average charged lepton energy for negative Λ_b polarization. In particular the value of polarization found in the data should correspond to an increase of $\langle E_l \rangle$ of about 0.5 GeV with respect to the unpolarized Monte Carlo. However, this is true only under the assumption that the Λ_b fragmentation function is identical in data and in the Monte Carlo. As argued in section 4.2 there is neither good experimental knowledge about the fragmentation to Λ_b nor a sufficiently precise theoretical prediction. Results of this analysis suggest a significant discrepancy between data and Monte Carlo. The value of $\langle E_l \rangle$ observed in data is almost 3σ lower than the one reconstructed in the unpolarized Monte Carlo (see Table 7). It indicates a significantly harder Λ_b fragmentation function in our simulation. In principle the presented measurement should not be sensitive to the Λ_b fragmentation function (see section 4.2). However, the experimental reality (i.e. selection cuts, efficiency functions, etc.) could introduce a certain limited dependence. The possible systematics introduced by this effect will be discussed in section 6.3.

6.2 Statistical error

The statistical error has the following sources:

1. statistical fluctuations in the lepton and neutrino energy spectra,
2. resolution on the neutrino energy,
3. correlation between lepton and neutrino energies in the Λ_b signal,
4. background fraction in *right-sign* event sample (f_{bck}),
5. statistical error on the y^{MC} evaluation.

Their individual contributions to the total statistical error are summarized in Table 8.

To estimate the statistical fluctuation of the charged lepton spectra we use an actual measurement of the lepton energy. From the shape (RMS) of the obtained lepton distribution (see Fig. 22) we evaluate the error on the average value to be equal to $5/\sqrt{N}$ GeV. In the case of the neutrino spectra the error has two sources. The first one is analogous to the one in the charged lepton sector. The second one comes from the finite resolution of the single neutrino energy reconstruction. The missing energy

source	$\sigma(R_y)$
spectra fluctuations	± 0.12
resolution on the neutrino energy	± 0.10
lepton–neutrino correlation	± 0.04
background fraction (f_{bck})	± 0.03
y^{MC} evaluation	$+0.03$
Total	$\mathbf{\pm 0.17}$

Table 8: Statistical error contributions.

reconstruction procedure has been discussed in section 5.5. For the error evaluation a momentum independent 4.5 GeV neutrino energy resolution has been assumed for both the Λ_b signal and the underlying background. The two sources contribute to a bigger apparent error on the average neutrino energy. The value found for the data amounts to $7.3/\sqrt{N}$ GeV. From the above two numbers we can derive the statistical fluctuation of the genuine neutrino spectrum in data. It amounts to $5.7/\sqrt{N}$ GeV.

There is an additional source of the statistical error induced on y. Energies of the charged lepton and neutrino in the signal are correlated via the $\Lambda_b^0 \rightarrow l\nu X_c$ decay dynamics. From the Λ_b Monte Carlo this correlation has been evaluated to be -29%. Since the correlation is negative, it will contribute to an enhancement of the final uncertainty on $y = \langle E_l \rangle / \langle E_\nu \rangle$.

The statistical error of the background fraction f_{bck} evaluation is also taken into account but has a minor contribution to the total statistical uncertainty.

6.3 Systematic uncertainties

The following sources of systematic error have been considered:

1. $BR(\Lambda_c^+ \rightarrow l\nu\Lambda^0 X)$
2. Λ_c^+ polarization
3. neutrino energy reconstruction (data – Monte Carlo discrepancy)
4. background bias (physical processes leading to the definite *sign* correlation)
5. contribution from $\Lambda_b \rightarrow \tau\nu_\tau X$ where the τ subsequently decays semileptonically.

6. Λ_b fragmentation function

7. theory — assumed value of (m_c/m_b) ratio

Their individual contributions to the total systematic uncertainty are summarized in Table 9.

source	$\sigma(R_y)$
$BR(\Lambda_c^+ \to l\nu\Lambda^0 X)$	± 0.048
Λ_c polarization	± 0.011
neutrino energy	± 0.043
background bias	± 0.040
$\Lambda_b \to \tau\nu_\tau X$ and $\tau \to \nu_\tau l \nu_l$	$+0.018$
Λ_b fragmentation function	$+0.027$
theory	± 0.005
Total	$\mathbf{+0.083}$ $\mathbf{-0.077}$

Table 9: Systematic error contributions.

As discussed in section 5.5 there is a large offset in the reconstructed neutrino energy when the Λ_c decays semileptonically. The offset is equal to the average energy of the escaping ν from the Λ_c decay which is $\approx$2.8 GeV. Therefore the result obviously depends on the fraction of Λ_c's decaying semileptonically. In the analysis it has been assumed that the apparent $R_{sl} = \frac{BR(\Lambda_c \to l\nu\Lambda^0 X)}{BR(\Lambda_c \to \Lambda^0 X)}$ after the whole analysis selection is equal to 16% according to the value found in the simulation. In fact there is a large uncertainty on this number. Most of it comes from the unknown BR($\Lambda_c \to \Lambda^0 X$) which is estimated to be $(35 \pm 11)\%$ [19]. Taking the PDG value for the BR($\Lambda_c \to l\nu\Lambda^0 X$) one gets $R_{sl} = (9^{+5}_{-4})\%$. On the other hand the process $\Lambda_c \to l\nu\Lambda^0 X$ should to a large extent saturate inclusive Λ_c semileptonic decays. Therefore, from the CLEO result on BR($\Lambda_c \to e^+ X$) = $(3.4 \pm 0.4)\%$ [83] we get an estimate of the upper limit on R_{sl} which is $R_{sl} = (19^{+8}_{-5})\%$. To account for this large uncertainty we varied $\frac{BR(\Lambda_c \to l\nu\Lambda^0 X)}{BR(\Lambda_c \to \Lambda^0 X)}$ by $\pm 8\%$ w.r.t. the 16% found in the simulation. This variation corresponds to a systematic shift of the measured missing energy of 220 MeV.

The Λ_c polarization can affect the average missing energy measurement in Λ_c semileptonic decays because the average energy of the neutrino escaping from Λ_c depends on the polarization. Fortunately, in the semileptonic decays of up-type quarks the neutrino is only slightly affected. In the matrix element for this process the charged lepton and neutrino swap their roles relative to the down-type quark decays [74]. Now the charged lepton has the maximal sensitivity to polarization and the neutrino retains only some 30% of it. Therefore, the expected neutrino energy variation under the unit polarization change does not exceed 12%. This leads to a systematic error on the average neutrino energy of 50 MeV.

As discussed in section 5.5, a systematic discrepancy between data and Monte Carlo in the hemisphere energy estimation should not fake the neutrino energy measurement by more than 200 MeV.

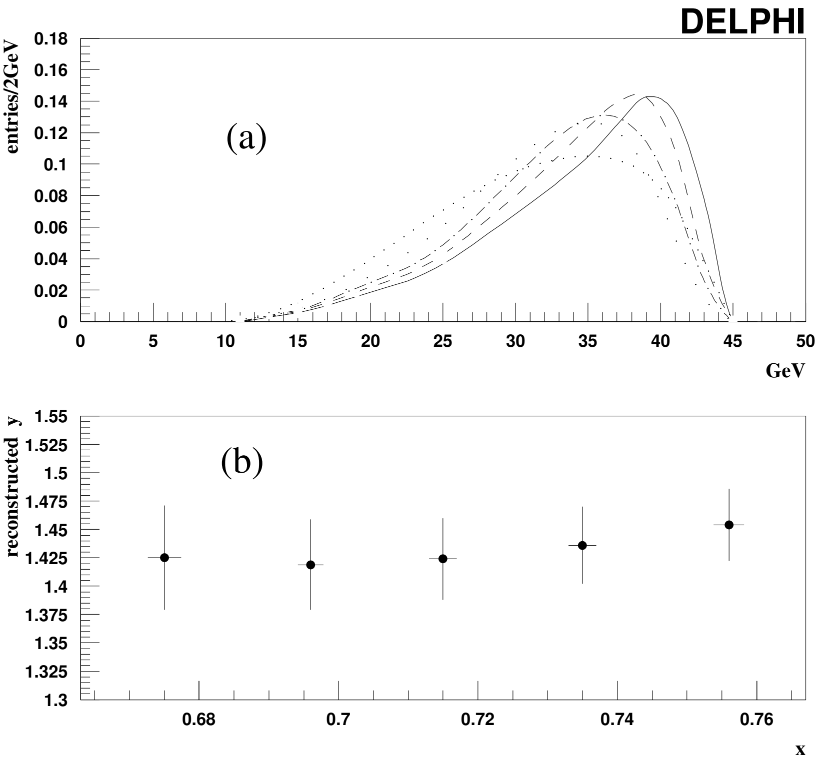

Figure 30: Dependence of the reconstructed y on the Λ_b fragmentation function in the background free Monte Carlo. Plot (a) shows five different Λ_b energy spectra used for this evaluation. Plot (b) shows corresponding reconstructed y values as a function of x = $\langle E_{\Lambda_b}/E_{\rm beam}\rangle$.

Possible differences between the *wrong-sign* sample and the *right-sign* background can lead to a shift in the measured Λ_b polarization. The shift comes both from a different effective y reconstructed in the two samples and their unequal population faking the apparent f_{bck}. As discussed in 5.3 there are several sources of such biases. Here we will consider contributions from semileptonic decays of c-baryons (from both b and c events) and semileptonic decays of B mesons where a prompt Λ^0 has been produced from the fragmentation. Λ_b decays into τ lepton will be discussed separately afterwards. As evaluated from the simulation, events where the selected lepton comes from the semileptonic decay of a Λ_c baryon should contribute to some 4% of the *wrong-sign* population. The two subclasses (b-baryon $\rightarrow$ c-baryon $\rightarrow l^+\nu_l\Lambda^0X$ and $c \rightarrow$ c-baryon $\rightarrow l^+\nu_l\Lambda^0X$) give similar contributions. Both are highly suppressed by the requirement of high $\mathrm{p_T}$ for the lepton candidate. Additionally, the first process leads to charged leptons of significantly lower momenta because of the cascade. A 3.0 GeV momentum cut already gives a remarkable reduction. The second process leads to energetic leptons but at the same time is suppressed by the cut on the b-tagging probability. A possible background bias coming from c-baryon decays (contribution to *wrong-sign*) is difficult to estimate. For the systematic error estimation we assume that the whole c-baryon sample is $\pm 100\%$ polarized and hence leads to extreme y values. As discussed in section 5.3 in our Monte Carlo one observes a significant excess of *right-sign* $\Lambda^0 l$ combinations originating from true leptons from semileptonic B decays paired with prompt Λ^0's from fragmentation. This effect comes from the strong energy ranking in the fragmentation model. Since we cannot a priori assume anything about the existence of this mechanism in reality we can only include its impact on the measured polarization into the systematic error. For the systematic error estimation we take the rate observed in the Monte Carlo where the asymmetry in the B meson sample corresponds to some 10% of the total background. The error evaluation is based on the assumption that the meson contribution carries no polarization. The effect of energy ranking in our Monte Carlo is asymmetric. However, since we know very little about the fragmentation in the real life we leave the corresponding error to be symmetric although it may lead to a small overestimation of the systematic error. To extract the final systematic error induced by all physical sources discussed above we add them incoherently. The summed error on R_y does not exceed 0.04.

The contribution from $\Lambda_b \rightarrow \tau\nu_\tau X$ with the subsequent decay $\tau \rightarrow \nu_\tau l \nu_l$ gives rise to the extra *right-sign* $\Lambda^0 l$ correlations. Its estimated fraction in the observed signal is small (<2%) but three escaping neutrinos associated with a low energy lepton from the τ cascade result in extremely low y. This background source might fake the observed R_y by -0.018.

From the average value of the reconstructed charged lepton spectrum $\langle E_l \rangle$ there is an indication of a harder Λ_b fragmentation in our Monte Carlo relative to the one observed in the real data. The possible influence of the fragmentation on the polarization measurement has been studied using the Λ_b enriched Monte Carlo. In the five subse-

sample	# of B^0 candidates	f_{bck}	$\langle E_l \rangle$ (GeV)	$\langle E_\nu \rangle$ (GeV)	y
MC $b\bar{b}$	557±8	0.054±0.010	10.63±0.26	7.08±0.29	1.50±0.07
data	281±7	0.088±0.017	10.79±0.38	7.02±0.43	1.54±0.11

Table 10: Polarization observables for the B^0 meson selection measured in data and in the simulation of $b\bar{b}$ events.

quent event samples the Λ_b fragmentation function was forced to be more and more soft in order to reproduce charged lepton mean energy observed in data. The corresponding shapes of the Λ_b spectra are shown in Fig. 30a. The resulting y behaviour presented in Fig. 30b shows a limited but perceptible impact of the Λ_b average energy on the measured polarization. Varying the Λ_b energy spectrum towards the lower energies by -11% ($\langle E_{\Lambda_b} \rangle$: 34.4 $\searrow$ 30.7 GeV) we observe a drop in the reconstructed R_y not bigger than 0.027.

The theoretical error arises mainly from the uncertainty on the value of m_c/m_b and is small. Varying m_c^2/m_b^2 in the large range between 0.04 and 0.13 we find a systematic error on R_y smaller than 0.005.

6.4 Consistency check using B mesons

As already argued in section 3.2 mesons should not retain any polarization of the primary b quark. The polarization measured on the B^0 sample should be consistent with zero. Therefore, an independent measurement of the B meson polarization can serve as a test of the analysis consistency. This cross-check is statistically limited, however, it could reveal possible large systematics in case they existed.

The B^0 meson sample was selected as described in 5.4 and contains 281 ± 7 B^0 candidates. The whole procedure to extract the polarization was identical with the one used in the Λ_b analysis. The neutrino energy reconstruction together with the fitted resolution is shown in Fig. 31. The better resolution comes from the fact that B^0 is quasi fully reconstructed in the channel $B^0 \to l\nu D^*(X)$. Figure 32 shows the lepton and neutrino reconstructed spectra for the D^*l events found in the real data. The polarization observables calculated according to formula 0.32 obtained for the B meson sample are summarized in Table 10. From there we obtain:

$$R_y^B = \frac{y^{data}}{y^{MC}} = 1.027 \pm 0.088 \qquad (0.38)$$

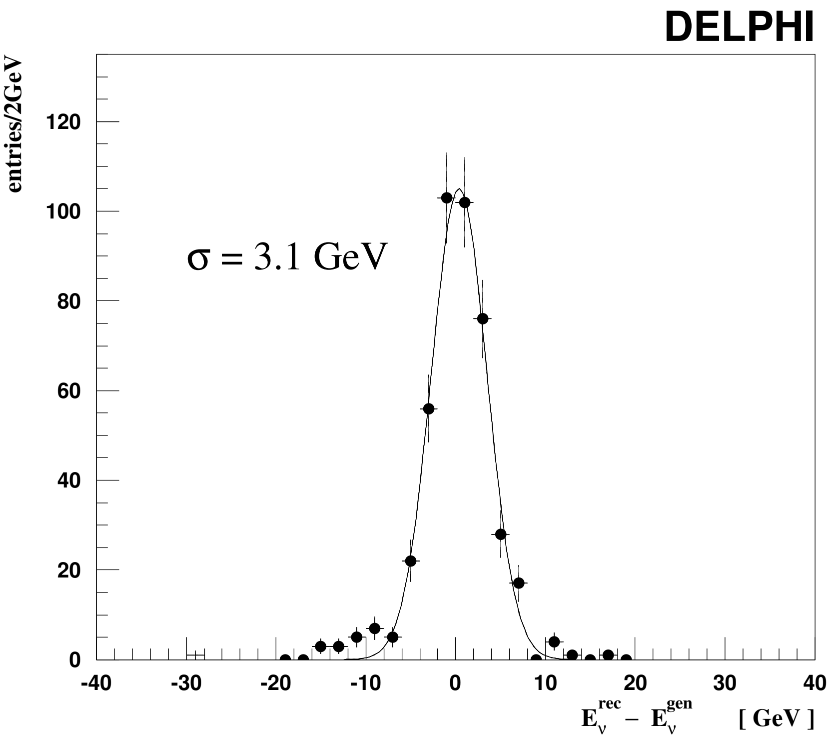

Figure 31: Final E_ν resolution obtained for Monte Carlo $B^0 \to l\nu D^*(X)$ events.

which corresponds to:

$$P_B = -0.07^{+0.23}_{-0.19} \qquad (0.39)$$

The quoted error is purely statistical. The result is compatible with zero polarization in the b-meson sector. Although the statistical significance of this result is limited it excludes the existence of a severe systematic discrepancy between data and MC in the missing energy estimation and proves the general correctness of the experimental procedure.

6.5 Comparison with the ALEPH measurement of P_{Λ_b}

The first Λ_b polarization measurement based on data collected in the years 1991-1994 was published by ALEPH collaboration [84]. The quoted result was $-0.23^{+0.24}_{-0.20}$(stat.)$^{+0.08}_{-0.07}$(syst.). In the ALEPH analysis an additional signal purification has been performed requiring a common vertex of the Λ^0, lepton and an extra π (from

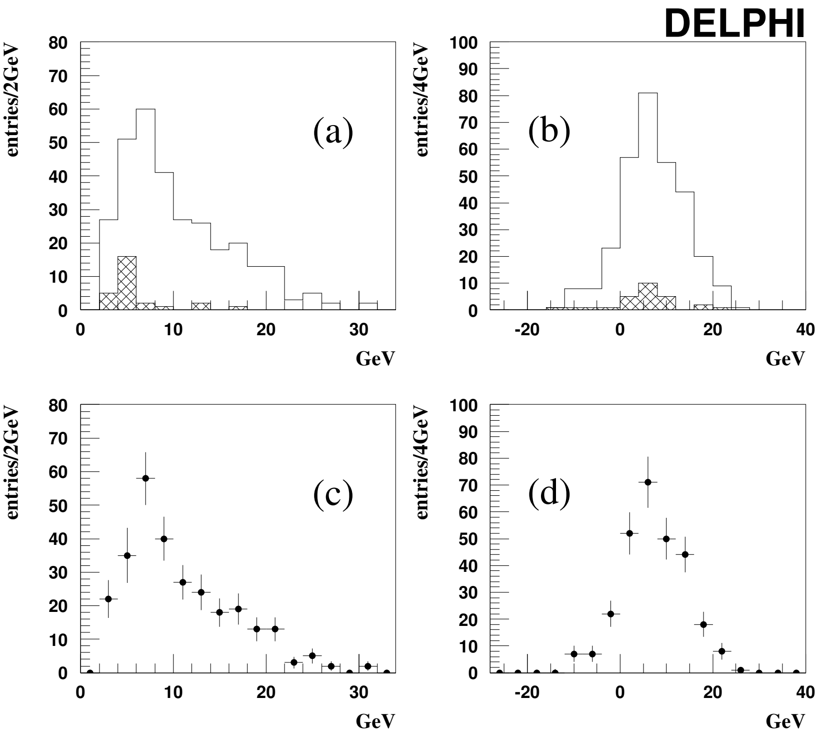

Figure 32: Lepton energy spectra for the D^*l sample found in data. Plots (a) and (c) show the charged lepton energy while plots (b) and (d) give corresponding distributions for the neutrino. The upper plots show energy distributions for *right-sign* (blank histogram) and *wrong-sign* (hatched histogram) D^*l pairs. The lower plots show the corresponding background subtracted spectra for the B^0 signal (*right-sign* $-$ *wrong-sign*).

Λ_c decay) with charge opposite to the Λ^0 baryon number. A year later the ALEPH measurement was updated to comprise all LEP1 statistics ($\approx$4 million Z^0) collected in the period 1991-1995 [85]. From this data sample 559$\pm$34 Λ_b candidates were selected using $(\Lambda^0\pi^+)l^-$ correlations. The conceptual novelty was the use of three different polarization observables proposed in [86]:

$$y_1 = \frac{\langle E_l \rangle}{\langle E_\nu \rangle},\ y_2 = \frac{\langle E_l^2 \rangle}{\langle E_\nu^2 \rangle} \text{ and } y_3 = \left\langle \frac{E_l}{E_\nu} \right\rangle$$

However, since the three variables are highly correlated only y_2 was chosen for extracting the final result. The ratio of the second order moments of the two spectra was found to give the best sensitivity to the Λ_b polarization. The polarization extracted using three different variables is shown in Fig. 33. The three curves give the experimental

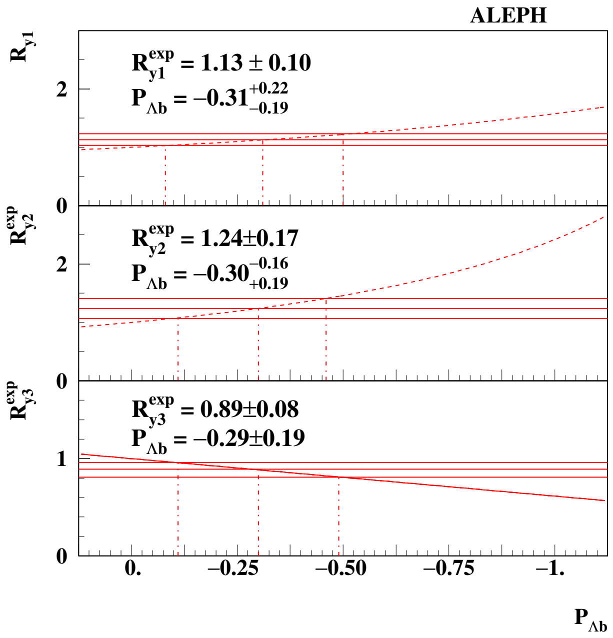

Figure 33: The procedure used to extract the polarization for the three different variables (ALEPH Collaboration [85]).

dependence of the three R_{y_i} $(i = 1, 2, 3)$ variables on Λ_b polarization. Horizontal lines represent the values obtained from the data together with the statistical error band. ALEPH determines the Λ_b polarization to be:

$$P_{\Lambda_b} = -0.30^{+0.19}_{-0.16}(\mathrm{stat.}) \pm 0.06(\mathrm{syst.})$$

The ALEPH and DELPHI results remaining compatible within the statistical uncertainty give evidence of either a high fraction of indirect Λ_b production through the heavier states $\Sigma^{(*)}$ or it may also point to yet not understood spin dynamics in the fragmentation and subsequent hadronization processes of $b \to \Lambda_b^0$. The implications of the measured polarization will be discussed in more detail in the following section.

The combined ALEPH $\oplus$ DELPHI result reads:

$$P_{\Lambda_b} = -0.36^{+0.17}_{-0.14}(\mathrm{stat.})^{+0.07}_{-0.06}(\mathrm{syst.})$$

In the presented analysis we have not used the y_2 observable to determine the polarization. The second moment of the energy spectrum is sensitive not only to its mean value but in particular to the distribution width. The energy resolution in data and in the simulation show some discrepancies (in data the RMS is typically ≈5% bigger) and hence might lead to considerable systematics not being under control at sufficient level. This approach, however, is worth further investigation in the future.

6.6 Implications of the result

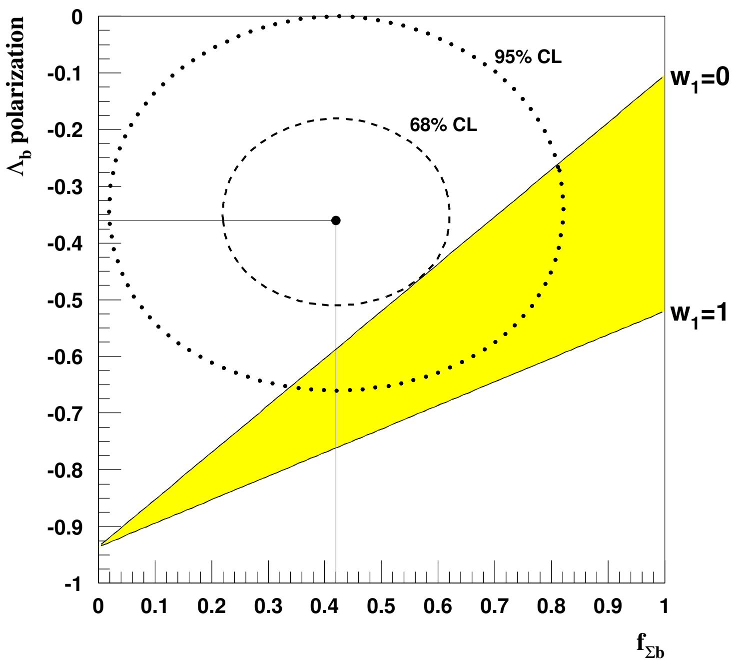

Figure 34: Measured value of the Λ_b polarization and $\Sigma_b^{(*)}$ production as compared to the theoretical prediction.

The low value of the measured polarization relative to the HQET expectation for the direct Λ_b production indicates a strong depolarization mechanism. The simplest explanation is based on the substantial contribution of the b quark fragmentation into Σ_b and Σ_b^* states which subsequently decay into a Λ_b: $b \to \Sigma_b^{(*)} \to \Lambda_b$.

Evidence for $\Sigma_b^{(*)}$ baryon production has been observed in the DELPHI experiment [52]. The measured production rate is $f(b \to \Sigma_b^{(*)}) = (4.8 \pm 1.6)\%$. When combined with an ALEPH estimate of inclusive b-baryon production
$f(b \to \text{baryons}) = (11.5 \pm 4.0)\%$ [87], this gives the fraction of $\Sigma_b^{(*)}$ in the total b-baryon

production $f_{\Sigma_b} = (42 \pm 20)\%$. Figure 34 compares the measured value of the Λ_b polarization and $\Sigma_b^{(*)}$ production with the theoretical predictions given in [72]. The latter depend on the w_1 parameter as discussed in section 3.3. Two bands $w_1 = 0$ and $w_1 = 1$ correspond to two extreme spin alignment cases: spin of the diquark is orthogonal to the fragmentation axis ($w_1 = 0$) and spin of the diquark is parallel to the fragmentation axis ($w_1 = 1$). Within the model in question the results clearly favour low w_1 values. The experimental results are at the limit of 1σ compatibility with the theoretical expectation for the extreme $w_1 = 0$. This observation remains in agreement with the direct w_1 measurement done in [52]. w_1 can be deduced from the angular distribution of the Σ^* production rate in the helicity frame. The value extracted from the fit to the pion angular distribution reads: $w_1 = -0.36 \pm 0.30 \pm 0.30$. Since negative values are unphysical, the result confirms the hypothesis of w_1 being close to zero. However, within the 95% confidence level the experiment stays in agreement with the theoretical model in a wide range of the w_1 parameter. We emphasize that the above depolarization prediction is valid only if the Σ_b and Σ_b^* are distinct resonances which seems to be the case according to the preliminary measurement of DELPHI.

A small diminution of the primary b quark polarization can be expected due to the value of the "effective coupling $\mathcal{A}_b$". $\mathcal{A}_b$ gives directly the mean b quark polarization from Z^0 decays as shown in formula (0.10). The experimental value of $\mathcal{A}_b$ determined from the forward-backward asymmetry $\mathrm{A_{FB}}$ turns out to lie somewhat lower than the uncorrected theoretical one. We have:
– Standard Model: $\mathcal{A}_b = 0.935$
– experiment (from $\mathrm{A_{FB}}$ [15]): $\mathcal{A}_b = 0.890 \pm 0.029$
Probably it would be justified to consider the latter number as the value of initial b polarization rather than the SM one.

Obviously, other not yet understood depolarization mechanisms occurring during hadronization cannot be a priori excluded.

7 Conclusions

The Standard Model predicts a high longitudinal polarization of b quarks produced at LEP in the reaction $e^+e^- \to Z^0 \to f\bar{f}$. It amounts to -0.94. Heavy Quark Effective Theory in turn predicts that in the direct fragmentation to a Λ_b baryon this high polarization should be transferred to the hadronic state without any loss. The experimental measurement of the Λ_b polarization at LEP gives important information about heavy quark hadronization and heavy baryon properties.

The Λ_b polarization has been measured using semileptonic decays selected from $\approx 3 \times 10^6$ hadronic Z^0 decays collected with the DELPHI detector between 1993 and 1995.

The Λ_b event selection is based on charge correlations in pairs of high p_T leptons and Λ^0 baryons found in the same event hemisphere. The final sample contains 271 ± 22 Λ_b candidates.

The ratio of the average energies of charged leptons and neutrinos from Λ_b decays is an experimental observable which is both highly sensitive to polarization and practically free from theoretical uncertainties. The ratio found in the data was normalized to the one extracted from the explicitly unpolarized Monte Carlo sample. This eliminates experimental uncertainties arising from the detector response and the selection cuts. Any deviation from 1.0 of the normalized ratio is attributed to the Λ_b polarization.

The measured value is:

$$P_{\Lambda_b} = -0.48\ ^{+0.35}_{-0.27}(\text{stat.})\ ^{+0.15}_{-0.13}(\text{syst.})$$

The statistical error dominates. However, the systematic uncertainty is also considerable mainly due to the unknown fraction of the semileptonic Λ_c decays ($\Lambda_c \to l\nu\Lambda^0 X$), uncertainty in the neutrino energy reconstruction and physical processes possibly biasing the background estimation.

The result is in good agreement with the one obtained by the ALEPH collaboration. Both results either indicate a high fraction of indirect Λ_b production through the Σ_b and Σ_b^* cascade or can point to depolarization mechanisms not yet predicted in the framework of HQET. The decisive answer will come with better statistical sensitivity to both Λ_b polarization and $\Sigma_b^{(*)}$ production rate.

Acknowledgments

First and foremost, I would like to express my particular thanks to my supervisor, Agnieszka Zalewska who has been supporting my efforts throughout all the years from the early idea of this analysis till the last correction of my manuscript. I would also like to acknowledge her assistance in promoting my work and in particular in helping me to get more scientific experience in good foreign laboratories.

My special thanks go to professor Krzysztof Rybicki for his constant professional attention to my work and its progress. I thank all members of the former PEDC for the nice atmosphere and their help in solving many big and small problems. I am particularly grateful to Tadeusz Lesiak, Bogdan Muryn and Henryk Palka for their constant will to consult everyday problems of physics analysis as well as to Andrzej Bożek, Pawel Jalocha, Zbyszek Natkaniec and Mariusz Witek for making the world of computers more friendly to me. Many thanks go to my room mate, Staszek Mikocki for his friendship and moral support helping me to overcome occasional crises in my struggle with the matter of physics.

I want to express my utmost gratitude to Marek Jeżabek whose motivating theoretical discussions were the driving force of this adventure.

I wish to thank many people at CERN for their everyday help and introducing me to the world of the frontier physics. In particular I thank the members of the DELPHI Microvertex Group for their friendship and hospitality. I would like to express my gratitude to Paula Collins for reading and correcting my manuscript. Special thanks go to Ugo Gasparini and the whole heavy-baryon working group for being to me an essential source of experimental experience and know-how. I thank also Michael Feindt, Patrick Roudeau, Daniel Treille and Wilbur Venus for their kind and encouraging attention to my work.

I am greatly indebted to professor Jürgen Drees and professor Mirco Mazzucato for their hospitality, kindness and support of my work. Many special thanks go to all my friends at the University of Wuppertal and University of Padua with whom I had privilege to collaborate. Their friendship and help enabled me to fully appreciate and profit from my stays in these two outstanding centers.

Finally, last but not least, I wish to thank my wife and my mother for their heart, understanding and being with me all the time.

The work has been partially supported by the KBN grants 2 P302 112 06 and 2 P303B 146 10.

Bibliography

[1] P. Brückman "Λ_b^0 Polarization at LEP", Acta.Phys.Pol.B26 (4): 813-817, 1995

[2] P. Brückman – DELPHI collab. "Λ_b polarisation in Z^0 decays", contribution to the 28th Int. Conf. on High Energy Physics, Warsaw, July 1996
and P. Brückman "Λ_b^0 Polarization at LEP", proceedings the 28th Int. Conf. on High Energy Physics, Warsaw, July 1996, Vol. I 910-913, World Scientific, Singapore

[3] Crowley-Milling,M C; "The worlds' largest accelerator: the electron-positron collider, LEP"; Proc. R.Soc.Lond., A:338 (1983)

[4] Bachy,G; Hofmann,A; Myers,S; Picasso,E; Plass,G; "The LEP Collider: construction, project status and outlook" Proc.of 14th Int. Conf. on High Energy Accelerators, Tsukuba, Japan, 22-26 Aug 1989, 16-33 (1990) 19-23

[5] LEP Performance WORKSHOPs; see e.g. proceedings of the Chamonix VII LEP Performance WORKSHOP, January 1997

[6] http://www.cern.ch/CERN/AreaMap.ps

[7] ALEPH Collab. "Preliminary results on Z^0 Production Cross Section and Lepton Forward-Backward Asymmetries using the 1990-1995 Data", proceedings of the 28th Int. Conf. on High Energy Physics, Warsaw, July 1996

[8] DELPHI Collab. "Precision determination of the Z^0 resonance parameters: and measurement of fermion pair production at LEP 1.5" contributed paper to the 28th Int. Conf. on High Energy Physics, Warsaw, July 1996

[9] L3 Collab. "Preliminary L3 Results on Electroweak Parameters using 1990-1995 Data", L3 note 1980, August 1996

[10] OPAL Collab. "A preliminary Update of the Z^0 Line Shape and Lepton Asymmetry Measurements with a Revised 1993-1994 LEP Energy and 1995 Lepton Asymmetry", OPAL physics note PN242, July 1996

[11] Richter,B; "The SLAC Linear Collider: the machine, the physics, and the future"; Particles and fields-1981: testing the standard model: Proc. C A Heusch and W T Kirk AIP, New York, (1982), 433-460

[12] Phinney,N; "The SLAC Linear Collider", subm. to 15th Int. Conf. on High Energy Accelerators, Hamburg, Germany, 20-24 Jul 1992, Proc. J Rossback Int. J Mod Phys.,A. Supl.: 2A-2B (1993) World Sci., Singapore, 1993

[13] D. Ward, "Tests of the Standard Model W mass and WWZ couplings", Plenary talk given at EPS-HEP'97 Conf., Jerusalem, August 1997

[14] M. Feindt, "B Physics", Plenary talk given at EPS-HEP'97 Conf., Jerusalem, August 1997

[15] K. Mönig, "Recent Results from LEP at the Z on Electroweak and Heavy Flavour", Invited talk given at the 24th SLAC Summer Institute on Particle Physics, August 1996

[16] The LEP Experiments: ALEPH, DELPHI, L3 and OPAL, "Combining Heavy Flavour Electroweak Measurements at LEP", Nucl. Instrum. Meth. Phys. Res., A:378 (1996) 101-115

[17] M. Feindt, "Heavy Quark Spectroscopy at LEP", proceedings of the 6th Int. Conf. on Hadron Spectroscopy, HADRON '95, Manchester, July 1995

[18] http://nicewww.cern.ch/sl/stat/lucompar.gif

[19] Particle Data Group, Review of particle physics, Phys. Rev. D 54, Part 1 (1996)

[20] P. Roudeau. "Heavy Flavor Physics at LEP", Plenary talk given at LP-HEP 91 Conf., Geneva, Switzerland, Jul 25 – Aug 1, 1991

[21] UA1 Collab. "First Observation of the Beauty Baryon Λ_b in the Decay Channel $\Lambda_b \to J/\Psi\ \Lambda_s$ at CERN Proton–Antiproton Collider", Phys.Lett.B273: 540-548, 1991

[22] ALEPH Collab., D.Decamp et al., "Evidence for b Baryons in Z^0 Decays", Phys.Lett.B278: 209, 1992

[23] OPAL Collab., P.D.Acton et al., "Evidence for b-flavoured Baryon Production in Z^0 Decays at LEP", Phys.Lett.B281: 394, 1992

[24] DELPHI Collab., P.Abreu et al., "Measurement of Λ_b production and lifetime in Z^0 hadronic decays", Phys.Lett.B311: 379, 1993

[25] DELPHI Collab. "Search for exclusive decays of the Λ_b baryon and measurement of its mass", Phys.Lett.B374: 351-361, 1996

[26] ALEPH Collab. "Measurement of the mass of the Λ_b baryon", Phys.Lett.B380: 442-452, 1996

[27] ALEPH Collab., D.Buskulic *et al.*, "Improved measurement of the B^0 and B^+ meson lifetimes", Z.Phys.,C: 71 (1996) 31

[28] CDF Collab., http;//www-cdf.fnal.gov/physics/new/bottom/bottom.html

[29] CDF Collab. F. Abe *et al.*, "Measurement of the B^- and $\bar{B}^0$ meson lifetimes using semileptonic decays", Phys.Rev.Lett.76: (1996) 4462

[30] DELPHI Collab. "Accurate measurement of the B_d^0 meson lifetime", contribution to the ICHEP'96 Conference, Warsaw, July 1996

[31] DELPHI Collab. P. Abreu *et al.*, "A Measurement of B^+ and B^0 Lifetimes using $\overline{\mathrm{D}}\ell^+$ events", Z.Phys.,C: 68 (1995) 13

[32] DELPHI Collab. W. Adam *et al.*, "Lifetimes of Charged and Neutral B Hadrons using Event Topology", Z.Phys.,C: 68 (1995) 363

[33] OPAL Collab. R. Akers *et al.*, "Improved measurements of the B_0 and B_+ meson lifetimes", Z.Phys.,C: 67 (1995) 379

[34] SLD Collab. "Measurement of the B^+ and B^0 Lifetimes from Semileptonic Decays at SLD", contributed paper to the 28th Int. Conf. on High Energy Physics, Warsaw, July 1996

[35] SLD Collab. "Measurement of the B^+ and B^0 Lifetimes with topological vertexing at SLD", contributed paper to the 28th Int. Conf. on High Energy Physics, Warsaw, July 1996

[36] ALEPH Collab., D.Buskulic *et al.*, "Study of the $\mathrm{B}_S^0\bar{\mathrm{B}}_S^0$ oscillation frequency using $\mathrm{D}_S^-\ell^+$ combinations in Z decays", Phys.Lett.B377: 205, 1996

[37] ALEPH Collab., D.Buskulic *et al.*, "Measurement of D_s^+ meson production in Z decays and of the $\overline{B}_s^0$ lifetime", Z.Phys.,C: 69 (1996) 585

[38] CDF Collab., "Measurement of the Lifetime of the B_s^0 Meson from $D_s l$ Correlation", contributed paper to the 28th Int. Conf. on High Energy Physics, Warsaw, July 1996

[39] CDF Collab. F. Abe *et al.*, "Measurement of the lifetime of the B_s^0 meson using the exclusive decay mode $B_s^0 \to J/\Psi\Phi$", Phys.Rev.Lett.77: 1945, 1996

[40] DELPHI Collab. "Mean Lifetime of the B_s^0 Meson", contributed paper to the 28th Int. Conf. on High Energy Physics, Warsaw, July 1996

[41] DELPHI Collab. P. Abreu *et al.*, "Mean lifetime of the B_s^0 meson", Z.Phys.,C: 71 (1996) 11

[42] OPAL Collab. R. Akers *et al.*, “An Improved Measurement of the B_S^0 Lifetime”, Phys.Lett.B350: 273, 1995

[43] ALEPH Collab. “Updated Measurement of the b Baryon lifetime”, contribution to the ICHEP’96 Conference, Warsaw, July 1996

[44] CDF Collab. F. Abe *et al.*, “Measurement of Λ_b^0 lifetime using $\Lambda_b^0 \to \Lambda_c^+ + l^- + \bar{\nu}$”, Phys.Rev.Lett.77: 1439, 1996

[45] DELPHI Collab. “Lifetime and production rate of beauty baryons from Z decays”, Z.Phys.,C: 68 (1995) 375-390

[46] DELPHI Collab. “Determination of the average lifetime of b-baryons”, Z.Phys.,C: 71 (1996) 199-210

[47] OPAL collab. “Measurement of the average b-baryon lifetime and the product branching ratio $f(b \to \Lambda_b) \times BR(\Lambda_b \to \Lambda l^- \bar{\nu} X)$”, Z.Phys.,C: 69 (1996) 195-214

[48] OPAL collab. “A measurement of the Λ_b^0 lifetime”, Phys.Lett.,B: 353 (1995) 402-412

[49] DELPHI Collab. “Production of strange b baryons decaying into $\Xi^{\mp} l^{\mp}$ pairs at LEP”, Z.Phys.C68: 541-554, 1995

[50] ALEPH Collab. “Strange b baryon production and lifetime in Z^0 decays”, Phys.Lett.B384: 449-460, 1996

[51] OPAL Collab., contribution eps0272, Brussels, 1995

[52] DELPHI Collab., M. Feindt, C. Kreuter, A. Miagkov, O. Podobrin “First Evidence for Σ_b and Σ_b^* Baryons”, DELPHI-95-107, contribution to the “EPS-HEP 95” Conference Brussels, 27th July - 2nd August 1995

[53] DELPHI Collab. “The DELPHI detector at LEP”, Nucl.Instrum.Methods A 303 (1991) 233-276

[54] DELPHI Collab. “Performance of the DELPHI Detector”, Nucl.Instrum.Methods A 378 (1996) 57-100

[55] DELPHI Vertex Detector group “The DELPHI Microvertex Detector”, Nucl.Instrum.Methods A 328 (1993) 447

[56] DELPHI Vertex Detector group “The DELPHI silicon strip microvertex detector with double sided readout”, Nucl.Instrum.Methods A 368 (1996) 413-432

[57] http://delphiwww.cern.ch/delfigs/export/detrgb.ps

[58] F. Halzen; A.D. Martin, "Quarks and leptons: an introductory course in modern particle physics", New York, Wiley, 1984

[59] P. Langacker, "W and Z physics", Invited talk given at China Center of Adv. Science & Technology Symp. on TeV Physics, Beijing, China, May 28 – Jun 8, 1990

[60] B. Mele & G. Altarelli "Lepton Spectra as a Measure of b quark polarization at LEP", Phys.Lett.B299: 345-350, 1993

[61] S. Jadach; Z. Was, "QED $O(\alpha^3)$ radiative corrections to the reaction $e^+e^- \to \tau^+\tau^-$ including spin and mass effects", Acta.Phys.Pol.B15: 1151-1184, 1984

[62] B. Mele "Lepton Spectra and the b Polarization at LEP" Mod.Phys.Lett.A9: 1239-1252, 1994

[63] ALEPH Collab., D.Buskulic *et al.*, "Improved Tau Polarisation Measurement", Z.Phys.,C: 69 (1996) 183

[64] DELPHI Collab. P. Abreu *et al.*, "Measurements of the τ Polarisation in Z^0 decays", Z.Phys.,C: 67 (1995) 183

[65] L3 Collab. O. Acciari *et al.*, "A Measurement of τ Polarization at LEP", Phys.Lett.B341: 245, 1994

[66] OPAL Collab. R. Akers *et al.*, "A Precise Measurement of the Tau Polarization and its Forward-Backward Asymmetry at LEP", Z.Phys.,C: 72 (1996) 365-375

[67] M. Neubert, "B Decays and the Heavy Quark Expansion"; CERN-TH-97-024, Feb. 1997; To appear in the Second Edition of Heavy Flavours, edited by A.J. Buras and M. Lindner (World Scientific, Singapore) and the references therein

[68] M. Neubert, "Heavy-Quark Effective Theory and Weak Matrix Elements", Plenary talk given at EPS-HEP'97 Conf., Jerusalem, August 1997

[69] T. Mannel & G. Schuler "Semileptonic Decays of Bottom Baryons at LEP", Phys.Lett.B279: 194-200, 1992

[70] F.E. Close, "An Introduction to Quarks and Partons", London Academic Press, 1979

[71] F.E. Close, J. Körner, R. Phillips and D. Summers "Heavy quark theory and b polarization at LEP", J.Phys. G 18 (1992)1716

[72] A.F. Falk & M.E. Peskin "Production, Decay and Polarization of Excited Heavy Hadrons", Phys.Rev.D49: 3320-3332, 1994

[73] J. Körner "Λ_b-Polarization from its Inclusive semileptonic Decay", Lectures given at Production and Decay of Hyperons CHarm and Beauty Hadrons, Strasbourg, France, September 1995 MZ-TH/95-33, Dec. 1995

[74] M. Jeżabek & J.H. Kühn "Lepton Spectra From Heavy Quark Decay", Nucl.Phys.B320: 20-44, 1989

[75] A. Czarnecki, M. Jeżabek, J.H. Kühn "Lepton Spectra From Decays of Polarized Top Quarks", Nucl.Phys.B351: 70-80, 1991

[76] A. Czarnecki et al. "QCD Corrections to Decays of Polarized Charm and Bottom Quarks", Phys.Rev.Lett.73: 384-387, 1994

[77] C.Bourdarios, P.Brückman, U.Gasparini, T.Lesiak – DELPHI Collab. "Determination of average b-baryon lifetime at LEP", contribution to the HEP'97 Conference, Jerusalem, August 1997

[78] G. Bonvicini & L. Randall "Optimized Variables for the Study of Λ_b Polarization", Phys.Rev.Lett.73: 392-395, 1994

[79] Sjöstrand,T; "PYTHIA 5.7 and JETSET 7.4: physics and manual", CERN-TH.7112/93 (revised February 1994), 1994

[80] G.V. Borisov "Lifetime Tag of events $Z^0 \to b\bar{b}$ with the DELPHI detector", DELPHI 94-125 PROG 208, 11 August, 1994

[81] C. Mariotti – private communication
& http://delphiwww.cern.ch/delfigs/export/ep_col_www.ps

[82] K. Hamacher – private communication

[83] CLEO Collab. "Study of the Decay $\Lambda_c^+ \to \Lambda l^+ \nu_l$" Phys.Lett.B323: 219-226, 1994

[84] ALEPH Collab. "Measurement of the Λ_b polarization in Z decays", Phys.Lett.B365: 367, 1996

[85] ALEPH collab. "A measurement of the Λ_b polarisation at LEP in Z decays", contribution to the 28th Int. Conf. on High Energy Physics, Warsaw, July 1996

[86] C. Diaconu, M. Talby, J. Körner & D. Pirjol "Improved variables for measuring the Λ_b polarization", Phys.Rev.D53: 6186-6194, June 1, 1996

[87] ALEPH Collab. "A measurement of the $|V_{cb}|$ from $\overline{B}^0 \to D^{*+} l^- \overline{\nu}_l$", Phys.Lett.B359: (1995) 236

List of Figures

1 CERN area map . . . 1
2 Layout of the DELPHI apparatus . . . 7
3 Decay of a polarized particle . . . 13
4 Principal electroweak vertices . . . 14
5 e^+e^- annihilation at LEP . . . 15
6 e^+e^- cross-section . . . 17
7 Primary fermion polarization . . . 18
8 Λ_b semileptonic decay . . . 22
9 Asymmetry coefficients α . . . 23
10 Theoretical behaviour of $\langle E_l \rangle$ and $\langle E_\nu \rangle$ . . . 28
11 Theoretical behaviour of the R_y variable . . . 29
12 Layout of the Λ_b event . . . 34
13 Λ^0 reconstruction in DELPHI . . . 35
14 b tagging performance in DELPHI . . . 37
15 Impact of the b tagging on the Λ_b signal . . . 39
16 Signal from the genuine Λ_b semileptonic decay . . . 40
17 Λ_b reconstruction efficiency . . . 41
18 Λ_b signal in data . . . 42
19 Λ_b signal in MC . . . 43
20 Signal composition . . . 45
21 Hadronization – a simplified picture . . . 46
22 l and ν energy spectra in data . . . 48
23 l and ν energy spectra in data . . . 49
24 B^0 signal in data . . . 51
25 B^0 signal in MC . . . 52
26 Neutrino energy resolution in Λ_b simulation . . . 53
27 Reconstructed versus generated ν energy . . . 54
28 Lepton and neutrino energy reconstruction in data and MC . . . 56
29 The result extraction . . . 60
30 Λ_b fragmentation systematics . . . 64
31 Neutrino energy resolution in B^0 simulation . . . 67
32 l and ν energy spectra in data ($D^* l$ sample) . . . 68
33 The ALEPH result . . . 69

34 Experimental results versus theoretical predictions 70

List of Tables

1 Data collected by DELPHI 12
2 c_V and c_A for different fermions 15
3 Monte Carlo composition of the *right-sign* and the *wrong-sign* event samples 44
4 *right-sign* and *wrong-sign* background in the Monte Carlo 47
5 Total visible event energy in the data and in the Monte Carlo 54
6 Hemisphere energy in data and in the Monte Carlo 57
7 Results obtained for the reference Λ_b Monte Carlo, the simulated unbiased $q\bar{q}$ events and the data 59
8 Statistical error contributions 62
9 Systematic error contributions 63
10 Polarization observables for the B^0 meson selection 66